

# Ice Shelves as Floating Channel Flows of Viscous Power-Law Fluids

Indranil Banik & Justas Dauparas

June 26, 2022

## Contents

<b>1</b>	<b>Introduction</b>	<b>3</b>
<b>2</b>	<b>Ice Tongues</b>	<b>4</b>
<b>3</b>	<b>Laterally Confined Ice Shelves</b>	<b>8</b>
<b>4</b>	<b>The Grounding Line</b>	<b>14</b>
4.1	No Sidewalls . . . . .	15
4.2	With Sidewalls . . . . .	18
<b>5</b>	<b>Experiments</b>	<b>19</b>
5.1	The setup . . . . .	19
5.2	1% aqueous xanthan solution . . . . .	23
5.3	0.5% aqueous xanthan solution . . . . .	25
5.4	Thickness Profile . . . . .	28
5.5	Particle Imaging Velocimetry . . . . .	29
5.6	No Sidewalls . . . . .	32
<b>6</b>	<b>Conclusions</b>	<b>36</b>
<b>A</b>	<b>The Effects of Ice Shelf Collapse</b>	<b>37</b>

## Abstract

We attempt to better understand the flow of marine ice sheets. Treating ice as a viscous shear-thinning power law fluid, we develop an asymptotic (late-time) theory in two cases - the presence or absence of contact with sidewalls. Most real-world situations fall somewhere between the two extreme cases considered.

The solution when sidewalls are absent is a fairly simple generalisation of that found by Robison. In this case, we obtain the equilibrium grounding line thickness using a simple computer model and have an analytic approximation.

For shelves in contact with sidewalls, we obtain an asymptotic theory, valid for long shelves. We determine when this is. Our theory is based on the velocity profile across the channel being a generalised version of Poiseuille flow, which works when lateral shear dominates the force balance.

We conducted experiments using a laboratory model for ice. This was a suspension of xanthan in water, at a concentration of 0.5% by mass. The lab model has  $n \approx 3.8$  (similar to that of ice). Our theories agreed extremely well with our experiments for all relevant parameters (front position, thickness profile, lateral velocity profile, longitudinal velocity gradient and grounding line thickness). We also saw detailed features similar to natural systems. Thus, we believe we have understood the dominant force balance in both types of ice shelf.

Our work has implications for the collapse of ice shelves, such as Larsen B. Lateral friction in the shelf provides significant buttressing, which can be removed if the shelf collapses. This would greatly accelerate the flow of ice and accelerate sea level rise. Our model allows a calculation of the magnitude of the effect based on the topography and the initial rate of flow, if such a collapse were to occur. However, for an ice tongue, sudden acceleration of this nature appears unlikely as there is no lateral friction.

# 1 Introduction

This paper builds on previous work by Robison on what are essentially ice tongues (shelves with no lateral confinement). We generalise this to fluids with arbitrary shear-thinning coefficient  $n$  (our theory should also work for shear-thickening fluids, but we did not perform experiments using such fluids). Then, we also attempt to generalise the result for laterally confined ice shelves, found by Pegler. The ice sheet is treated as a classical viscous gravity current, though we need to be careful about when this is a valid assumption.

In this paper, we start with a first principles theoretical solution to shelves without sidewalls in the case of constant initial thickness. Reasons for expecting the initial thickness to be constant are also given. Then, we derive a similarity solution for a laterally confined shelf in a channel of constant width. The solution is valid in the asymptotic limit, so we also derive roughly where this is.

The sheet is also briefly reviewed, so that we can address the grounding line. The equilibrium grounding line thickness is found for ice tongues. For laterally confined ice shelves, we already have the initial thickness and thus the grounding line position without considering the sheet. We briefly discuss how the sheet may influence the dynamics, noting that it does not in the asymptotic limit.

We describe experiments we conducted to help us develop these theories and to test them. The experiments with 1% concentration xanthan are described first, for the case of sidewall contact. Then, the effect of lowering the concentration is shown. Data for experiments in which there was no sidewall contact are also shown, and compared with theoretical predictions for the grounding line thickness. An important point is that there are artefacts of our experimental setup, due to the way the flow is initialised. We determine the length over which such effects are dissipated. Fortunately, the sheet was longer than this length.

As well as the position of the propagating front, we also have the velocity field in the shelf and sheet. The methods used to obtain this data and the results are discussed and compared with theoretical expectations. The thickness of the shelf as a function of position (the profile) is also shown from a photograph, and compared with our model.

Using our newly developed understanding, we give a partial explanation of the effect of an ice shelf collapsing on the rate of flow of the associated ice sheet. This should be treated with some caution at this stage, but can readily explain large increases in the flow rate over short time intervals (such as occurred with Larsen B). Our work suggests that such a phenomenon can only occur in ice shelves significantly affected by sidewall contact, something which is easily checked. Our model allows a rough calculation of the magnitude of the effect if a particular ice shelf were to collapse, based on topography and other data. However, our work does not shed much light on which shelves are likely to actually collapse.

## 2 Ice Tongues

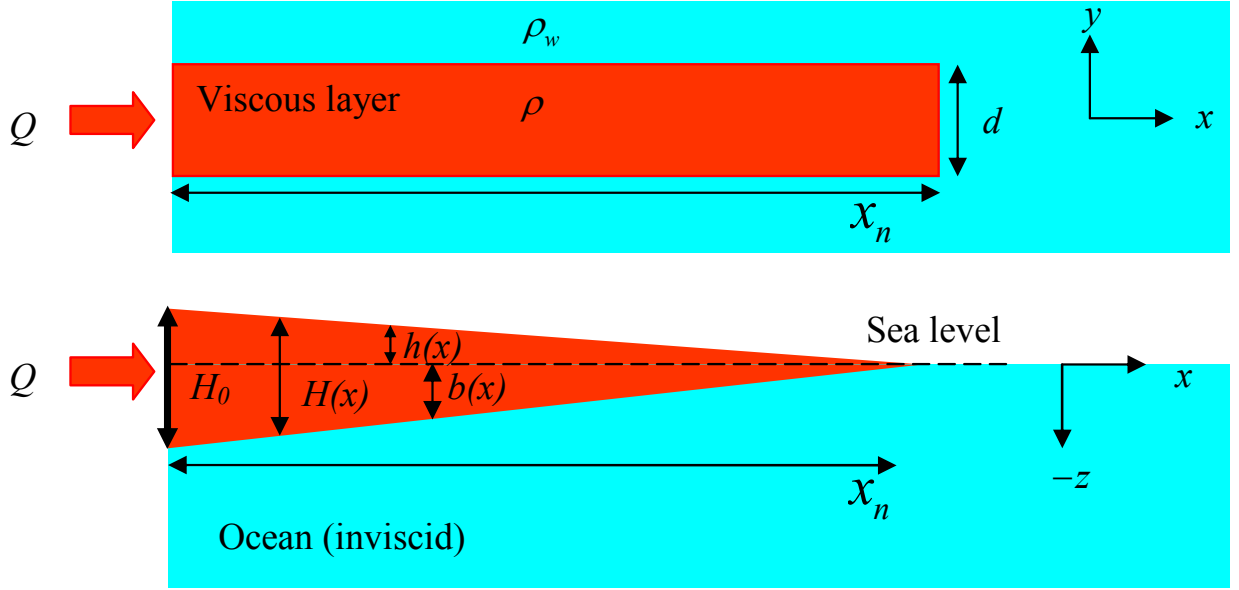


Figure 1: Plan and side views of the situation considered.

We consider the flow of an incompressible viscous fluid (at low Reynolds number) according to the geometry shown in Figure 1 (with  $Q$  held constant) and assume that the flow does not spread laterally. Although the width of the flow probably could be determined based on  $Q$  and other parameters, we do not attempt to do this. Instead, we treat the width of the shelf as an independent variable.

The force balance in the  $x$ -direction is that

$$\frac{\partial}{\partial x} \int_{-b}^h \sigma_{xx} dz = -\rho_w g b \frac{\partial b}{\partial x} \quad (1)$$

because there are no lateral or vertical stresses and water pressure has a component in the  $x$ -direction (because the normal to the shelf does). We neglect lateral flow and assume that  $H' \ll 1$  so that  $w \ll u$  (vertical flow negligible). Because the value of the above integral at the front of the shelf must balance with the integrated hydrostatic pressure of the ocean, we have (see Robison et al) that

$$\int_{-b}^h \sigma_{xx} dz = -\frac{1}{2} \rho_w g b^2 = -\frac{1}{2} \rho g H b, \text{ because } \rho_w b = \rho H \text{ (Archimedes)} \quad (2)$$

Considering the absence of lateral and vertical shear in this system, our model for the viscosity is

$$\eta = \eta_o \left( \frac{\partial u}{\partial x} \right)^{\frac{1}{n}-1} \quad (3)$$

Writing that

$$\sigma_{xx} \equiv -P + 2\eta \frac{\partial u}{\partial x} \quad (4)$$

and applying a vertical balance of forces argument (using also  $\frac{\partial w}{\partial z} = -\frac{\partial u}{\partial x}$ ) we obtain that

$$\sigma_{xx} = -\rho g(h - z) + 4\eta \frac{\partial u}{\partial x} \quad (5)$$

Integrating this vertically, we get that

$$-\frac{1}{2}\rho g H^2 + \int 4\eta \frac{\partial u}{\partial x} dz = -\frac{1}{2}\rho g H b \quad (6)$$

$$4\eta_o \int \left( \frac{\partial u}{\partial x} \right)^{\frac{1}{n}} dz = \frac{1}{2}\rho g H(H - b) \quad (7)$$

$$= \frac{1}{2}\rho g' H^2 \text{ because } h \equiv \frac{g'}{g} H \quad (8)$$

The term  $g'$  is called the reduced gravity, and accounts for the fact that only a fraction of the shelf is above the waterline. Thus, gradients in the height above sea level are smaller than gradients in  $H$ . Applying Archimedes' Principle to the shelf, we get that

$$\frac{g'}{g} = \frac{\rho_w - \rho}{\rho_w} \quad (9)$$

Continuing with our derivation,

$$\eta_o \left( \frac{\partial u}{\partial x} \right)^{\frac{1}{n}} H = \frac{\rho g' H^2}{8} \quad (10)$$

$$\frac{\partial u}{\partial x} = \left( \frac{\rho g' H}{8\eta_o} \right)^n \quad (11)$$

As this is positive, we note that  $u > 0$  throughout the shelf. Now, we use this information inside the continuity equation:

$$d^{-1} \frac{\partial H}{\partial t} + H \frac{\partial u}{\partial x} + u \frac{\partial H}{\partial x} = 0 \quad (12)$$

We use a Lagrangian picture to better visualise the situation.

$$d^{-1} \frac{DH}{Dt} = -H \frac{\partial u}{\partial x} \quad (13)$$

$$= -H^{n+1} \alpha \text{ where } \alpha \equiv \left( \frac{\rho g'}{8\eta_o} \right)^n \text{ is constant.} \quad (14)$$

In the co-moving (Lagrangian) frame, each fluid element enters the shelf at time  $t_0$ . Assuming that  $H(t_0)$  is independent of  $t$  (i.e. a constant source thickness), we must have that  $H = H(t - t_0)$  only. This means that  $\frac{\partial u}{\partial x}|_t = f(t - t_0)$ . Therefore,

$$u(x, t) = u_0 + \int_0^x f(t - t_0) dx' \quad (15)$$

$$= u_0 + \int_0^x f(\tau(x')) dx' \text{ where } \tau \equiv t - t_0 \text{ and } \tau = 0 \text{ for } x = 0 \quad (16)$$

We now convert the integral required to obtain  $u$  from one over  $x$  to one over  $\tau$ . The value of  $\tau$  is 0 when  $x = 0$ . When the fluid element reaches  $x$ ,  $\tau = t - t_0$ . We note that a fluid element injected at the source

over a time interval  $d\tau$  has a total volume  $Q d\tau$ . At all later times, it occupies the same volume. However, it is also a part of the profile. This means that it occupies a volume  $Hd dx$ . Thus,

$$u(t_0, t) = u_0 + \int_0^{t-t_0} f(\tau) \frac{dx'}{d\tau} d\tau \quad (17)$$

$$= u_0 + \int_0^{t-t_0} f(\tau) \frac{Q}{H(\tau)d} d\tau \quad (18)$$

This means that  $u$  is a function of  $(t - t_0)$  only, as we know that  $H$  is and  $u_0 = \frac{Q}{H_0 d}$  is assumed constant. Integrating  $u$  and assuming that the source of the shelf (a grounding line) remains static, we see that  $x$  is also going to be a function of  $t - t_0$  only. All fluid elements reach a given  $x$  at the same value of  $\tau$ . Thus, at that position,  $H$  is always the same (after the front has reached this position). We therefore have a steady profile.

Under these conditions, the continuity equation reduces to

$$u = \frac{Q}{Hd} \quad (19)$$

Differentiating this with respect to  $x$  and substituting in Equation 11, we obtain a first-order differential equation for the profile. Solving this subject to the constant initial thickness  $H_0$ , we get that.

$$H = \left[ \frac{Q}{(n+1)\alpha d} \right]^{\frac{1}{n+1}} (x+L)^{-\frac{1}{n+1}} \quad (20)$$

$$u = \left( \frac{Q}{d} \right)^{\frac{n}{n+1}} [(n+1)\alpha d]^{\frac{1}{n+1}} (x+L)^{\frac{1}{n+1}} \quad (21)$$

The constants  $L$  and  $\alpha$  are defined below:

$$L = \frac{Q}{(n+1)\alpha d H_0^{n+1}} \alpha \equiv \left( \frac{\rho g'}{8\eta_o} \right)^n \quad (22)$$

When  $x_n \ll L$ , the profile is essentially flat and the speed equals the initial value ( $\frac{Q}{H_0 d}$ ). For  $x_n \gg L$ , we have that

$$H \sim x^{-\frac{1}{n+1}} \quad (23)$$

(with  $u \sim x^{\frac{1}{n+1}}$ ). Finally, the position of the front as a function of time is readily determined from the velocity field.

$$x_n = \frac{Q}{(n+1)\alpha H_0^{n+1} d} \left[ (1 + \alpha n H_0^n t)^{\frac{1}{n} + 1} - 1 \right] \quad (24)$$

Alternatively, we could ensure the area enclosed by the profile upstream of the front is correct. As the profile is steady, this entails solving

$$\int_0^{x_n(t)} H(x) dx = \frac{Qt}{d} \quad (25)$$

Of course, both approaches agree for all  $n$ . For the case of  $n = 1$ , our solution reduces to that found by Robison et al in 2010.

In a real system, the shelf would be fed by a sheet at a grounding line (the ‘source’). The thickness here completely determines the buttressing exerted on the sheet and also affects the velocity field in the sheet. There is likely to be a unique thickness at which the forces at the grounding line are in equilibrium. Once this is attained, there is no further tendency for change (as the buttressing is independent of how far the front has propagated - it is always  $\frac{1}{2}\rho g' H_0^2$ ). We assume that the equilibrium so attained is stable. The equilibrium grounding line thickness is calculated in Section 4.1, although perturbations are not considered in this work.

### 3 Laterally Confined Ice Shelves

The geometry in this situation is the same as that considered before, except that now the half-width of the shelf rather than the full width is  $d$ . The major difference is the presence of laterally confining sidewalls, which we assume the shelf is in contact with at all times.

The effect of sidewalls will dominate over the effects of hydrostatic pressure on an ice shelf if the shelf is long enough relative to its width and height. To get an estimate for when this may be the case, we determine when the shelf starts thickening. In order for this to happen, the velocity field must be altered, so that instead of  $\frac{\partial u}{\partial x} > 0$ , we instead have  $\frac{\partial u}{\partial x} < 0$ . This means that, rather than continuity forcing the shelf to thin with distance, the front is going slower than fluid elements behind it so that the flow essentially piles up. We expect this to occur in order to provide a pressure gradient to overcome the viscous drag from sidewalls and keep the shelf flowing.

The key thing is that  $\sigma_{xx}$  is not purely hydrostatic pressure. There is a difference between pressure from xanthan and that from water (partly due to their different densities). This is balanced with a non-zero value of  $\frac{\partial u}{\partial x}$ . As we have seen, this is (initially) positive.

Now, if we were to reduce  $\sigma_{xx}$  enough that  $\frac{\partial u}{\partial x}$  were forced to become negative, then the situation would indeed be different to the no sidewalls scenario. To achieve this, a certain amount of drag from sidewalls is required. Note that  $\frac{\partial \sigma_{xx}}{\partial x} + \frac{\partial \sigma_{xy}}{\partial y} = 0$ . For  $y > 0$ ,  $\frac{\partial u}{\partial y} < 0$  so  $\sigma_{xy} < 0$ . Noting that the surface  $y = 0$  is free by symmetry, we see that  $\frac{\partial \sigma_{xy}}{\partial y} < 0$ , this also holding for  $y < 0$ . Thus,  $\frac{\partial \sigma_{xx}}{\partial x} > 0$ . Assuming  $H$  is not yet altered (so neither is  $\frac{\partial u}{\partial x}$  at the front), this means that  $\frac{\partial u}{\partial x}$  at the source eventually goes negative and becomes increasingly so. Once this occurs, the front starts decelerating and the shelf will be forced to start thickening.

As before, the initial value of that part of  $\sigma_{xx}$  which created a  $\frac{\partial u}{\partial x}$  term is  $\frac{1}{2}\rho g' H^2$  (when integrated vertically) - see Equation 4. Thus, for the shelf to start thickening, the total force from sidewalls must exceed the lateral integral of the above term (the total non-hydrostatic force, or pushing force). This way, there will no longer be any pushing force at all. With an even longer shelf and even more drag, it will change sign, making  $\frac{\partial u}{\partial x} < 0$ . We assume that this is a good indicator of when sidewalls start to have a significant impact upon the dynamics of the flow.

$$\frac{1}{2}\rho g' H^2 . 2d = \eta_0 \left( \frac{1}{2} \frac{\partial u}{\partial y} \right)^{\frac{1}{n}-1} \left( \frac{\partial u}{\partial y} \right) . 2LH \quad (26)$$

Henceforth, if we raise a negative number to a power, we mean that the absolute value of the number is raised to that power. *The end result is always positive.* For the viscosity, we have assumed that  $u = 0$  along the walls, so only lateral variations contribute to the total strain there. As a rough estimate, we assume a triangular velocity profile which gives

$$\frac{\partial u}{\partial y} = \frac{2\bar{u}}{d} \quad (27)$$

This is an underestimate because the boundary layer is probably very thin so has more shear. Using also the fact that  $\bar{u} = \frac{Q}{2Hd}$ , we obtain that

$$L = \frac{\rho g' H^{1+\frac{1}{n}} d^{1+\frac{2}{n}}}{2^{2-\frac{1}{n}} \eta_0 Q^{\frac{1}{n}}} \quad (28)$$

We note that  $\frac{\partial u}{\partial x}$  is very small in the asymptotic limit, because the shelf will get longer and longer (while the start of the shelf gets thicker, so  $u$  there decreases). As the force balance equation must always hold, we expect (treating  $\sigma_{xx}$  as purely hydrostatic) that the above equation linking  $L$  and some typical (e.g. maximum) thickness should hold in the asymptotic limit, when our approximation that  $\frac{\partial u}{\partial x}$  is very small becomes accurate. Essentially, we have balanced the hydrostatic pressure discontinuity not with a  $\frac{\partial u}{\partial x}$  term but instead with a  $\frac{\partial u}{\partial y}$  term. This suggests that the system may be self-similar at late times.



We have said that  $x_n \gg L$  is required for sidewalls to dominate the shelf, but assuming that a solution is discovered valid for such situations, when does this solution first become an accurate description of the length of the shelf? One probably needs computer simulations to answer this in detail, but here we give a rough idea. The shelf can not be longer than the solution predicts, because then  $|H'|$  is even lower so there is insufficient driving force to overcome viscous drag from the sidewalls. Also, even more drag exists than in the solution, because the shelf is even longer. So the situation can not arise.

However, the shelf can be shorter than our solution predicts - to compensate for the lower drag, it can simply be thick at the front, reducing the thickness gradient. So we see that there is no problem with a shelf shorter than the solution predicts, but a major problem with longer shelves - these can't exist (if the force balance is dominated by sidewalls). Thus, one way to determine  $L$  may be to find when continuing to apply the no sidewalls (basically, constant  $u$ ) solution leads to the front being further ahead than the yet to be derived solution when sidewalls dominate. Because this situation is impossible, we can use this to determine the point at which the no sidewalls solution can no longer be applied to the system. This approach would require determining the initial thickness of the shelf, which is possible under some circumstances (see Section 4.1).

We begin by using the fundamental equation for the balance of forces along the channel.

$$\frac{\partial \sigma_{xx}}{\partial x} + \frac{\partial \sigma_{xy}}{\partial y} = 0 \quad (29)$$

We assume that  $\frac{\partial u}{\partial x} \ll \frac{\partial u}{\partial y}$  over the vast majority of the channel, because the shelf is much longer than it is wide. This allows us to consider only lateral stresses. Also assuming negligible transverse and vertical velocities and no lateral variations in thickness, we obtain that

$$\frac{\partial}{\partial y} \left[ \eta_o \left( \frac{1}{2} \frac{\partial u}{\partial y} \right)^{\frac{1}{n}-1} \frac{\partial u}{\partial y} \right] = \rho g' \frac{\partial H}{\partial x} \quad (30)$$

Notice that only gradients in  $H$  can affect the velocity field, because the resulting pressure gradients *alone* drive the flow. Integrating the above equation with respect to  $y$  and applying the no-slip boundary condition for  $y = \pm d$  as well as no lateral stress along the centreline of the channel due to symmetry (i.e.  $\frac{\partial u}{\partial y} = 0$  for  $y = 0$ ), we obtain the velocity profile:

$$u = \frac{2^{1-n}}{n+1} \left( \frac{\rho g' H'}{\eta_o} \right)^n (d^{n+1} - y^{n+1}) \quad \text{where } H' \equiv \frac{\partial H}{\partial x} \quad (31)$$

A flow with a velocity pattern like this we shall call a generalised Poiseuille flow. The flux crossing a plane of constant  $x$  is easily found to be

$$q(x) = 2H \int_0^d u \, dy \quad (32)$$

$$= \frac{2^{2-n}}{n+2} \left( \frac{\rho g'}{\eta_o} \right)^n d^{n+2} (HH'^n) \quad (33)$$

The continuity equation can now be applied to obtain a single non-linear diffusion equation for the fluid.

$$\frac{\partial H}{\partial t} + \frac{2^{1-n} d^{n+1}}{n+2} \left( \frac{\rho g'}{\eta_o} \right)^n (HH'^n)' = 0 \quad (34)$$

For a more complicated geometry, a computer simulation will be required to understand what happens, although future work on simple geometries and on slowly varying  $d$  could shed some light on the problem. For such work, the  $d^{n+1}$  term should be brought inside the last bracket, to allow for the possibility that the width of the channel varies with position. For now,  $d$  is constant.

We now apply a scaling argument to the above equation and also to the equation of global mass conservation

$$\int_0^{x_n(t)} H(x) dx = \frac{Qt}{2d} \quad (35)$$

This suggests that the following quantity is a dimensionless constant of order 1:

$$\frac{x_n(n+2)^{\frac{1}{2n+1}} 2^{\frac{2n-1}{2n+1}}}{t^{\frac{n+1}{2n+1}} d^{\frac{1}{2n+1}} Q^{\frac{n}{2n+1}}} \left( \frac{\eta_o}{\rho g'} \right)^{\frac{n}{2n+1}} \quad (36)$$

We look for a solution in terms of the similarity variable

$$\varepsilon = \frac{x(n+2)^{\frac{1}{2n+1}} 2^{\frac{2n-1}{2n+1}}}{t^{\frac{n+1}{2n+1}} d^{\frac{1}{2n+1}} Q^{\frac{n}{2n+1}}} \left( \frac{\eta_o}{\rho g'} \right)^{\frac{n}{2n+1}} \quad (37)$$

Our analysis indicates that this is directly proportional to  $\frac{x}{x_n}$ . Because  $x_n$  rises slower than  $t$ , the fact that the area enclosed by the profile must rise linearly with time implies that the whole profile must also be thickening. Thus,  $H$  will necessarily have an explicit dependence on  $t$ . Using the fact that  $H \sim \frac{Qt}{2dx_n}$ , we obtain that

$$H = \frac{(n+2)^{\frac{1}{2n+1}} Q^{\frac{n+1}{2n+1}} t^{\frac{n}{2n+1}}}{2^{\frac{2}{2n+1}} d^{\frac{2n+2}{2n+1}}} \left( \frac{\eta_o}{\rho g'} \right)^{\frac{n}{2n+1}} \psi(\varepsilon) \quad (38)$$

where  $\psi(\varepsilon)$  (the dimensionless profile) is of order 1 near the source and decreases to 0 at the front.

Differentials in  $x$  and  $t$  can be converted into differentials in  $\varepsilon$ , applying the usual chain rule. Such an analysis shows that the powers of all externally imposed parameters are indeed equal on all terms, so that we may obtain a single ordinary differential equation for the profile (in terms of similarity co-ordinates).

$$(\psi\psi'^n)' = -\frac{n}{2n+1}\psi(\varepsilon) + \frac{n+1}{2n+1}\varepsilon\psi'(\varepsilon) \quad (39)$$

$$\int_0^{\varepsilon_n} \psi(\varepsilon) d\varepsilon = 1 \quad (40)$$

$$\psi\psi'^n = 1 \text{ at } \varepsilon = 0 \quad (41)$$

The term  $\psi\psi'^n$  corresponds to the (dimensionless) flux crossing a given position. This gradually decreases from its initial value. The reason is that part of it is 'lost along the way' because it goes into increasing the thickness of the profile.

In the real system, the advance of the front is not driven by the requirement to push flux through it (unlike in ice tongues). It is in fact driven by the velocity of fluid elements at the front (because  $H' \neq 0$ ).

We obtain approximate expressions for  $\psi'$  that become exact at either end of the profile. Near the source (or the rear) of the profile,

$$\psi' \approx -\left( \frac{1}{\psi(0)} \right)^{\frac{1}{n}} \quad (42)$$

Near the front (at  $\varepsilon_n$ ), we may obtain a first integral of Equation 39 to deduce that

$$\psi' \approx -\left( \frac{n+1}{2n+1} \varepsilon \right)^{\frac{1}{n}} \quad (43)$$

We have used the fact that the integral of  $\psi$  with respect to  $\varepsilon$  (from the front to a point nearby) is second order in the value of  $\psi$ , as the profile is approximately triangular in this region (a singularity in  $H'$  leads to a singular velocity profile, so  $H'$  must be finite). Using these results, we may obtain an expression for the total change in  $\psi'$  over the profile, giving directly the fractional change in velocity along the profile (because  $u \propto \psi'^n$ ) - though we need the actual value of  $\varepsilon_n$  to compute this.

We solved the differential equation numerically by shooting backwards from the front, using as boundary conditions  $\psi = 0$  at  $\varepsilon = \varepsilon_n$  and the above expression for  $\psi'$ . Due to computing errors, there is a small error in  $\psi\psi'^n$  at the source, but none at the front of the profile. Obviously, errors near the source are much preferred, because  $\psi\psi'^n = 0$  at the front (so we can ill afford errors here).

Although the solution looks reasonable for almost any value of  $\varepsilon_n$ , only one value can actually make the total area enclosed by the profile equal to 1. An estimate for the error made by the computer can then be obtained by checking how far off the solution is from satisfying Equation 41.

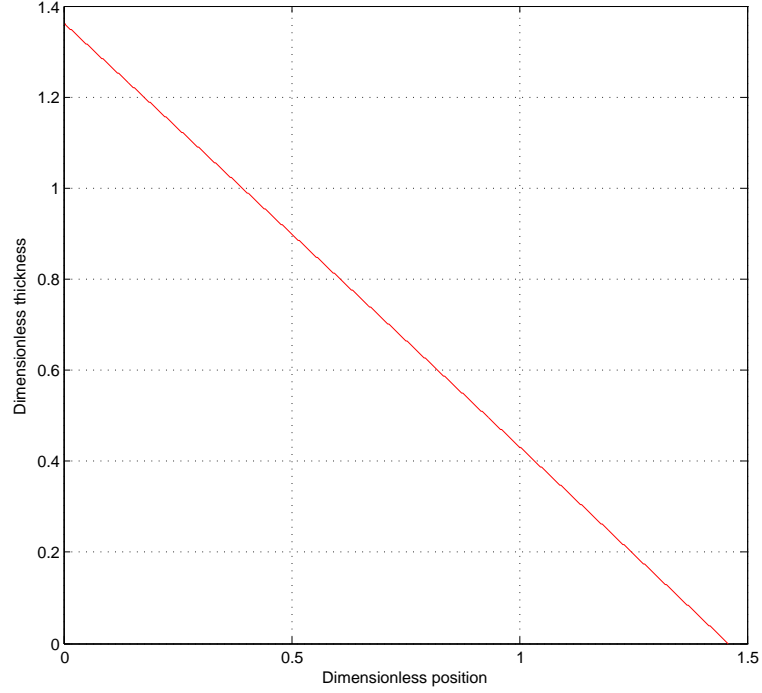


Figure 2: Dimensionless profile for  $n = 3.8$ . We promise we didn't just draw a triangle!

Amazingly, the whole profile is very nearly triangular. However, the slope does steepen by about 3% for  $n = 3.8$ . At higher  $n$ , this effect is reduced and both sides have length approaching  $\sqrt{2}$ . The reason is that  $\psi\psi'^n$  always goes from 1 to 0, and as  $\psi \neq 0$  (except right at the front), we must have that

$$\psi' \rightarrow 1 \forall \varepsilon \text{ as } n \rightarrow \infty \quad (44)$$

We note briefly that for  $n = 0$ , the dimensionless profile is the unit square.

$n$	$\psi(0)$	$\varepsilon_n$	Fractional change in $u$
3.6	1.362	1.461	11.6%
3.8	1.364	1.460	11.1%
5.0	1.374	1.452	8.8%
5.2	1.375	1.451	8.5%
$\infty$	1.414	1.414	0

Table 1: Results of computer simulations for those values of  $n$  used in our experiments, and nearby values consistent with the error in  $n$ . Also included is the result for  $n = \infty$ .

The expressions for the front position and the source thickness of the profile as functions of time are:

$$x_n = \frac{t^{\frac{n+1}{2n+1}} d^{\frac{1}{2n+1}} Q^{\frac{n}{2n+1}} \left( \frac{\rho g'}{\eta_o} \right)^{\frac{n}{2n+1}}}{(n+2)^{\frac{1}{2n+1}} 2^{\frac{n-1}{2n+1}}} \varepsilon_n \quad (45)$$

$$H_0 = \frac{t^{\frac{n}{2n+1}} (n+2)^{\frac{1}{2n+1}} Q^{\frac{n+1}{2n+1}} \left( \frac{\eta_o}{\rho g'} \right)^{\frac{n}{2n+1}}}{2^{\frac{n+2}{2n+1}} d^{\frac{2n+2}{2n+1}}} \psi(0) \quad (46)$$

Notice that the gradient of the profile decreases with time (i.e.  $H_0$  grows slower than  $x_n$ ). This is to keep the entry flux the same, despite a greater thickness (forcing a reduction in  $u$  and thus  $|H'|$ ).

As we have seen, thickening of the shelf is a hallmark of it being affected by viscous drag from sidewalls. For this to *dominate*, we need to allow significant thickening of the shelf. However, at a length of  $L$ , it will only just have started to thicken, so sidewalls will only dominate when  $x_n \gg L$ . We expect convergence to be slow because it takes some time for the transient to die down (the decay is  $x_n^{-1}$ ). This is because we assume that a section of shelf of length  $L$  is unaffected by sidewalls, so it is outside our model (and creates something akin to a shift in position measurements). This region is essentially flat (for realistic parameters) - see Figure 8 - because the force balance was different when this region crossed the source. The shelf behaves essentially as a solid body ( $\frac{\partial u}{\partial x}$  is very small), so the result of this earlier time remains permanently imprinted upon the shelf. For our solution to work well, we need this region to be a very small part of the entire shelf. This way, the last vestiges of the times when sidewalls were unimportant will have faded into insignificance.

Although we have estimated what length of shelf is required for sidewalls to dominate the system, this alone will not guarantee the similarity solution being accurate. This is because, even if the force balance was dominated by lateral friction from confining sidewalls, the amount of longitudinal stress *inherent to our solution* could still be very large, making it internally inconsistent.

The difference in  $u$  from the source to the front is approximately 10% (for  $n = 4$ ), so

$$\frac{\partial u}{\partial x} \approx \frac{u}{10x_n} \quad (47)$$

Obviously, there will be a region close to the centreline of the channel where  $\frac{\partial u}{\partial x} > \frac{\partial u}{\partial y}$ , but as long as this region is small, our solution should be accurate. For this to occur, we compare  $\frac{\partial u}{\partial x}$  along the centreline of the channel with  $\frac{\partial u}{\partial y}$  at the sidewalls (i.e. we compare maximum values). For  $n = 4$ , this leads to the requirement that

$$\frac{u}{10x_n} \ll \frac{4u}{d} \quad (48)$$

The conclusion, not altogether unexpected, is that the shelf needs to have a minimum aspect ratio. If we wish for  $\frac{\partial u}{\partial y}$  close to the sidewalls to be at least 10 times larger than  $\frac{\partial u}{\partial x}$ , then the shelf only needs to be half as long as the full width of the channel! Thus, the similarity solution is internally consistent for very short shelves. However, it does need to be much longer than  $L$ , and we believe that this is usually the stricter condition (it certainly was in our experiments).

We now touch briefly upon the effect of variations in thickness across the channel. In this case, a first integral of Equation 30 will no longer simply be directly proportional to  $y$ . Assuming the thickness is smaller near the sidewalls, then this will be a convex function. Therefore,  $\frac{\partial u}{\partial y}$  will be greater than before, for the same average  $H$  and  $H'$ . The effect of this can be determined by multiplying the formula for  $q(x)$  by a factor greater than 1.

However, the effect on the position of the front will be smaller than it might at first appear. Although the front must be further ahead than without the lateral thickness variation, this will also reduce the thickness and (combined with higher  $x_n$ ), will reduce  $|H'|$ . Therefore, the fractional increase in  $x_n$  (at the same value of  $t$ ) is only  $\frac{1}{2n+1}$  times as much as the fractional change in  $q$ . Thus, as long as the sidewalls are able to maintain the no-slip condition (i.e. as long as contact is not lost altogether), we expect the effect of lateral thickness variations on the front position to be small.

## 4 The Grounding Line

We now introduce a sloped bed at an angle of inclination of  $\alpha$ . The waterline is just above the top of this slope, with the weir just above the waterline. We now have both a sheet and a shelf, with the two linked at a grounding line. All parameters used previously still have the same meaning, except  $d$ . This is once again used for the full width of the shelf. A  $_G$  subscript is used to denote parameter values at the grounding line.

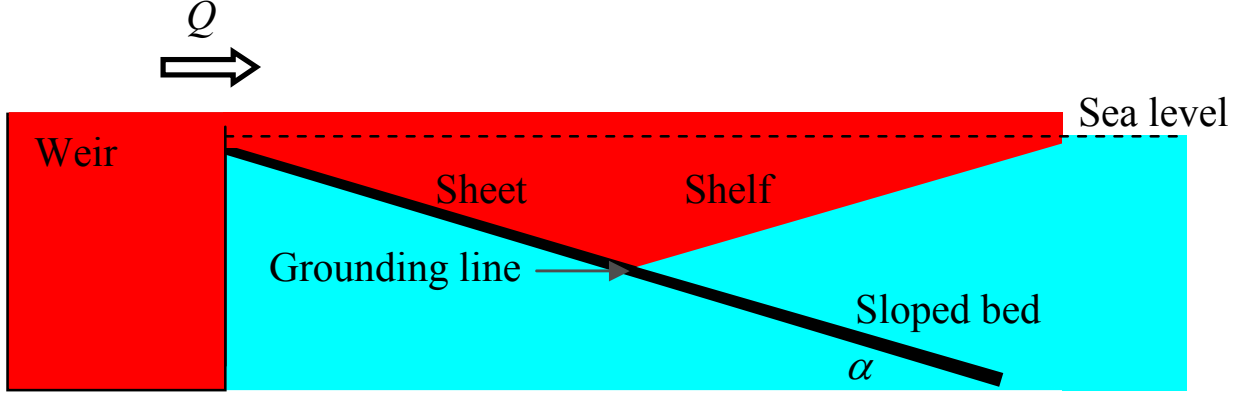


Figure 3: Side view of a channel flow with a grounding line.

We model the grounded portion of the viscous layer (the sheet) as a viscous gravity current. We prove later that this is valid. We also believe it to be valid in most natural situations, but can not confirm this.

Assuming that  $H \ll d$  (or that there are no sidewalls), we get that

$$\frac{\partial \sigma_{xx}}{\partial x} + \frac{\partial \sigma_{xz}}{\partial z} = 0 \quad (49)$$

The assumption of a viscous gravity current is formally equivalent to approximating the  $\frac{\partial \sigma_{xx}}{\partial x}$  term as a hydrostatic pressure gradient. Therefore, we get that

$$\frac{\partial}{\partial z} \left( \eta \frac{\partial u}{\partial z} \right) = \rho g h' \quad (50)$$

Solving the above equation subject to no slip at the base ( $z = -b$ ) and a free upper surface ( $\frac{\partial u}{\partial z} = 0$  at  $z = h$ ), we obtain the velocity profile for the sheet:

$$u(x, z) = \left( \frac{\rho g h'}{\eta_o} \right)^n \frac{2^{1-n}}{n+1} \left[ H^{n+1} - (h-z)^{n+1} \right] \quad (51)$$

The flux crossing given a plane of constant  $x$  is readily found to be:

$$q(x) = d \left( \frac{\rho g h'}{\eta_o} \right)^n \frac{2^{1-n}}{n+2} H^{n+2} \quad (52)$$

Note the similarity of the above equations with the corresponding ones for the shelf (with sidewalls). The confining surface runs parallel to the driving force, but in one case it is underneath and in another it is to either side. The shelf has no free surface like the sheet, but in the shelf the centreline of the channel acts as a free surface due to symmetry. Thus, we see that there is no fundamental difference between an ice sheet and an ice shelf confined by sidewalls both have gravity balancing viscous drag and they also have similar boundary conditions, leading to a similar velocity profile.

## 4.1 No Sidewalls

We solve first for the case where the shelf is not in contact with sidewalls. We assume that the flow does not spread laterally very much, or that it does so only over a very small region near the weir but not near the grounding line or in the shelf (so the width is constant in the regions we now discuss). We also assume that the grounding line has already reached its equilibrium position, so that conditions in the sheet close to this point are steady. In this case, we can set  $q = Q$  near the grounding line.

The fundamental force balance at the grounding line is for the force exerted on the water-facing side of the fluid in the  $x$ -direction. This is because such a force can not be transmitted anywhere except into the shelf. Therefore, it must balance with the same force in the shelf (where it is created by hydrostatic pressure of the ocean). In other words, we require continuity of  $\int_{-b}^h \sigma_{xx} dz$  across the grounding line.

In the sheet, there is a contribution from hydrostatic pressure of  $\frac{1}{2}\rho g H^2$ . However, it is not balanced by the normal stress in the shelf ( $\frac{1}{2}\rho_w g b^2$ ). The difference is  $\frac{1}{2}\rho g' H^2$ . This must be accounted for by *non-hydrostatic* forces in the sheet. Using the usual balance of vertical forces argument along with conservation of mass, we get that

$$I \equiv \int_{-b}^h 4\eta \frac{\partial u}{\partial x} dz = \frac{1}{2}\rho g' H^2 \text{ at the grounding line} \quad (53)$$

The pushing force ( $I$ ) is calculated directly from the velocity profile in Equation 51. We determine  $I$  numerically given a particular value of  $H$ . The value of  $h'$  is fixed by the requirement that conditions in the sheet near the grounding line be steady (i.e.  $q = Q$ ). Once  $h'$  is found, the computer next determines  $\frac{\partial u}{\partial x}$  and  $\frac{\partial u}{\partial z}$  as functions of  $z$  at the grounding line, using also  $H' = h' + \alpha$ . The equilibrium thickness of the grounding line is then given by varying  $H$  so as to make the integral on the left equal the expression on the right.

The viscosity is affected by both vertical and horizontal shear. Without horizontal shear, the integral will diverge for  $n > 2$ , assuming a non-zero value of  $\frac{\partial u}{\partial x}$  near the free upper surface. Thus, we use

$$\eta = \eta_o \left[ \sqrt{\left(\frac{\partial u}{\partial x}\right)^2 + \frac{1}{4}\left(\frac{\partial u}{\partial z}\right)^2} \right]^{\frac{1}{n}-1} \quad (54)$$

The flow in the sheet is dominated by vertical shear, which vanishes at the free upper surface. For a shear-thinning fluid, the viscosity is thus greatest near this surface. Here,  $u$  is also greatest. Thus, both  $\eta$  and  $\frac{\partial u}{\partial x}$  will be greatest here. This means that  $I$  is only really affected by the value of  $\frac{\partial u}{\partial x}$  near the upper surface.

The vertical velocity profile in the sheet has a thin boundary layer (for large  $n$ ), so in order to have flux conservation we must approximately have that  $u = \frac{Q}{Hd}$  outside this region. Thus, we expect that  $I$  will change sign when  $H'$  changes sign (i.e. when  $h' = -\alpha$ ). At the corresponding value of  $H$ ,  $I$  should be very small.

Computer simulations indicate that, for  $H$  fairly close to the ‘right’ value but not exactly equal to it,  $I$  is very sensitive to  $H$ . Thus, the value of  $H$  which makes Equation 53 hold and the value of  $H$  which makes the integral 0 are often quite close. This is equivalent to saying that the pushing force can easily be made quite large, compared with the hydrostatic pressure discontinuity. Thus, solving  $I = 0$  is approximately the right thing to do.

This suggests that the grounding line thickness may be approximated by assuming that  $h' = -\alpha$  there, so that

$$H_G \approx \left[ \frac{Q(n+2)}{d} \right]^{\frac{1}{n+2}} \left( \frac{\eta_o}{\rho g \alpha} \right)^{\frac{n}{n+2}} 2^{\frac{n-1}{n+2}} \quad (55)$$

Notice that  $g'$  is irrelevant if this approximation is accurate. The above equation requires  $H' = 0$ , but it does not actually result in  $I = 0$ . Because conditions remain the same if we move parallel to the sloped bed, moving along  $x$  at fixed  $z$  will lead to a geometric effect whereby

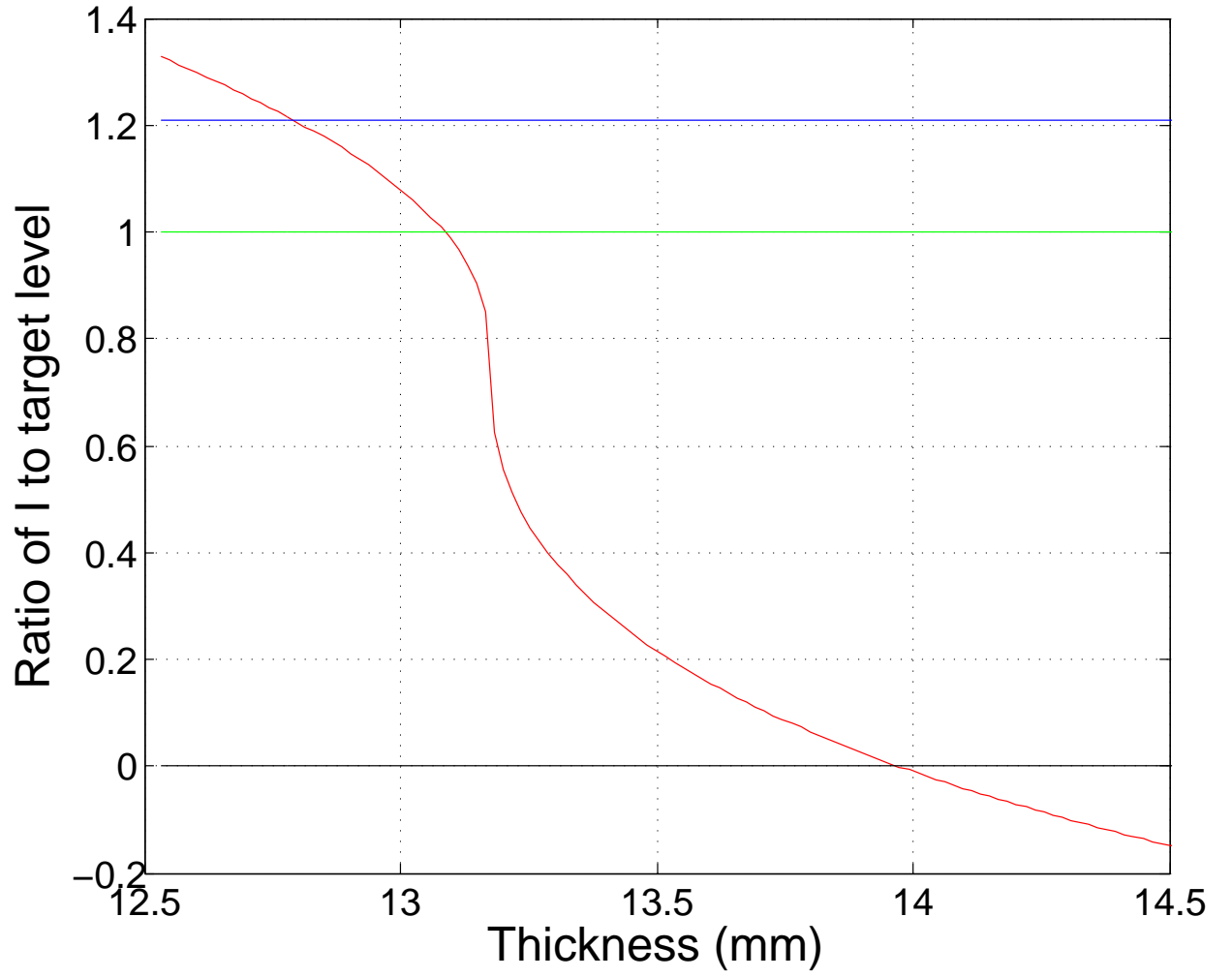


Figure 4: For parameter values matching those of one of our experiments,  $I$  divided by the hydrostatic pressure discontinuity is shown as the red curve. The green line is at 1. However, the intersection of the blue line with the curve is a good approximation. The location of this point is given in Equation 55.

$$\frac{\partial u}{\partial x} = \alpha \frac{\partial u}{\partial z} \quad (56)$$



Thus, the value of  $I$  divided by the hydrostatic pressure discontinuity is not exactly 0. It is:

$$2^{1\frac{1}{n}}\alpha^2\left(\alpha^2 + \frac{1}{4}\right)^{\frac{1}{2}\left(\frac{1}{n}-1\right)}\frac{g}{g'} \quad (57)$$

If this is close to 1, then Equation 55 will be a good approximation to the result of a full computer simulation (and the ice will be running nearly parallel to the sloped bed). A ratio above 1 means that Equation 55 underestimates  $H_G$  (as in Figure 4). For ice in sea water, we note that the equation holds exactly when  $\alpha = 9^\circ$ .

We warn the reader to check this ratio and the results of the computer simulation, to see what sign the error resulting from using Equation 55 is and whether its magnitude is acceptable. For now, the system is sufficiently simple that the full simulation only takes a few minutes. In more complicated systems, having a simple equation for the grounding line thickness may prove to be valuable, even if it is inexact.

Note that the green line will appear closer to the black line at very low  $g'$  (and further for higher  $g'$ ), whereas the blue line will appear not to move.  $g'$  does matter. As expected, a less buoyant fluid will have a thicker grounding line. Interestingly, though, reductions in  $g'$  can not raise the grounding line thickness above a certain value (although increases in  $g'$  can lower  $H_G$  without limit).

## 4.2 With Sidewalls

The essential difference in the presence of sidewalls (assuming they dominate the system) is that, once a shelf with a particular grounding line thickness is formed, there *is* a tendency for this thickness to change. Sidewall friction causes fluid to essentially ‘pile up’ behind the front to some extent, not just to flow completely freely as it does in the case of no sidewalls.

This ‘piling up’ means that there is *no* stable grounding line thickness. Therefore, the shelf thickens for ever. However, there is still a dynamic balance at the grounding line. This is because if all the flux entered the shelf, then it would want the grounding line thickness to increase at a certain rate. However, the sheet retains no flux, so it can’t grow. Thus, the grounding line can not advance.

The impossibility of the situation reveals what must really happen: part of the flux is retained by the sheet, allowing the grounding line to advance; while part goes into the shelf, presumably an amount equal to that which causes  $H_0$  to increase by precisely the rate at which the flux retained by the sheet allows. This means that there is a balance between dynamic conditions in the shelf (how much it wants to thicken, given the flux entering it) and kinematic conditions in the sheet (how much it must expand, given that it retains the flux not entering the shelf).

Eventually, the flux entering the shelf approaches  $Q$ . This is because the flux retained by the sheet is approximately equal to  $H_G \dot{x}_G$ , where a time derivative is indicated. Of course, for a fixed angle sloped bed we have that  $\dot{x}_G \propto \dot{H}_G$ . Considering that  $H_G \propto t^{\frac{n}{2n+1}}$ , we see that  $H_G \dot{H}_G \propto t^{-\frac{1}{2n+1}}$ . Thus, the flux retained by the sheet inevitably goes down to 0, but fairly slowly. This means that, even with a grounding line, the shelf will eventually converge to the similarity solution we found earlier (whether we consider the length of the shelf only, or the position of the front). The slow convergence may mean that in a real laterally confined ice shelf, it needs to be fairly long in order for all the flux to enter the shelf.

Ultimately, if one is interested in what happens before convergence has occurred, a computer simulation will be required. This will need to solve our non-linear diffusion equation for the shelf and a similar version for the sheet. The boundary condition must be that flux not entering the shelf is retained by the sheet (and may go into causing grounding line advance). Similar models have already been devised for Newtonian fluids.

We assume that the grounding line rapidly reaches a thickness such that  $|h'| \ll \alpha$ , so that  $H' \approx \alpha$ . This lets us approximate that

$$\frac{\partial u}{\partial x} \approx -\frac{Q}{H^2 d} \alpha \quad (58)$$

As there will be something like an extra power of  $H$  in the total pushing force exerted by the sheet (to account for the vertical integration), we see that this scales with time inversely to  $H$ .

In the shelf, we have that

$$\frac{\partial u}{\partial x} \approx \frac{Q}{H d x_n} \quad (59)$$

Hydrostatic pressure of the ocean is of course completely dissipated by sidewall friction. The pushing force in the shelf will also need to have an extra power of  $H$ , so this scales with time inversely to  $x_n$ . We expect this to grow faster than  $H$ , on the basis of our similarity solution for the shelf (which the system converges to, eventually). Thus, in the end, the pushing force from the sheet will always exceed that from the shelf.

The force balance at the grounding line still needs to hold. Now,  $\sigma_{xx} \equiv -P + 2\eta \frac{\partial u}{\partial x}$ , so  $P$  needs to be greater in the shelf than in the sheet. We believe this to mean that there is a sharp increase in  $H$  immediately after the grounding line, with this sudden change in  $H$  accounting for the discrepancy in the vertically integrated pushing force that we have just found. However, the effect becomes negligible in the asymptotic limit. We never noticed such an effect in any of our experiments, suggesting that it may be irrelevant.

## 5 Experiments

### 5.1 The setup

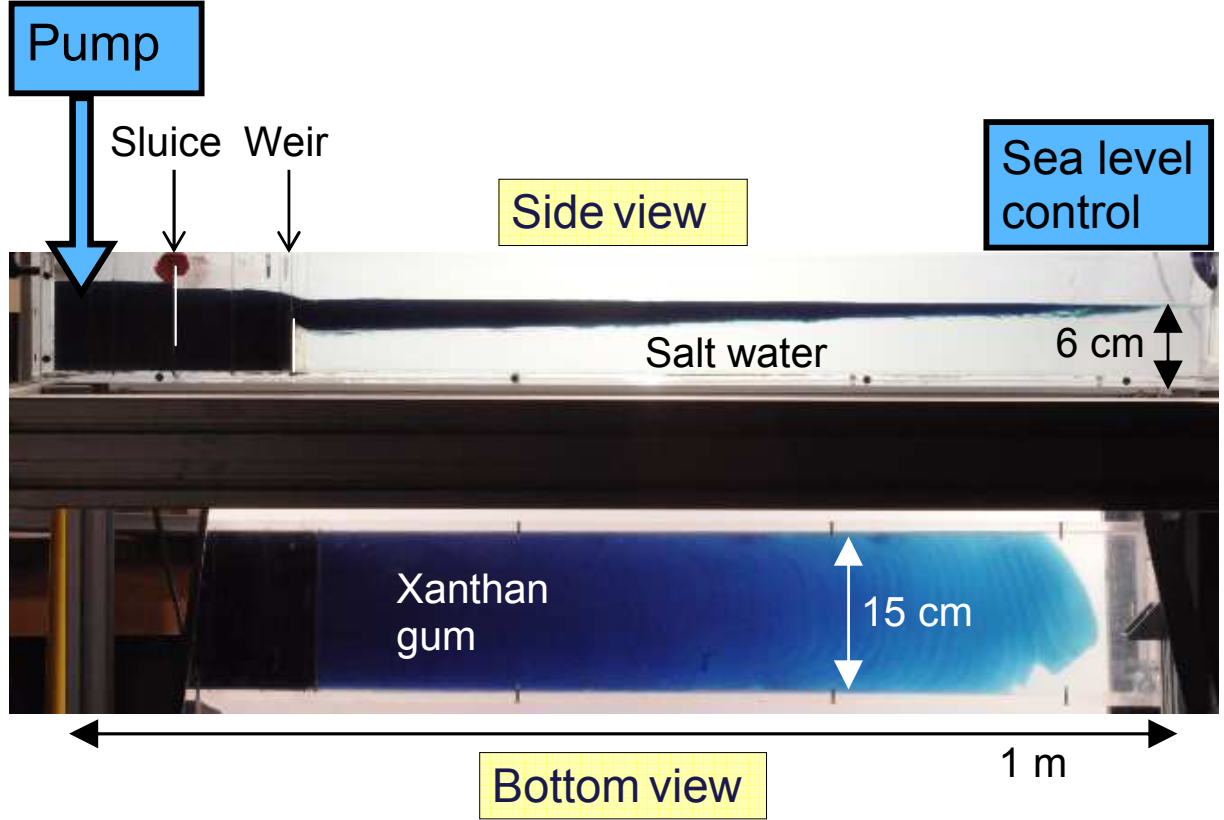


Figure 5: The experimental apparatus used (distances approximate). The bottom view is acquired using a mirror at  $45^\circ$  to the horizontal. A sloped bed was sometimes installed immediately after the weir (as shown in Figure 3)

The basic apparatus is shown in Figure 5. A peristaltic pump was used to maintain a constant flux into the region behind the sluice. The viscous fluid used was an aqueous suspension of xanthan gum at concentrations of 0.5% and 1% (by mass). Xanthan is a shear-thinning organic polymer. Salt was added to the ocean to increase its density.

The viscous fluid was overflowing the weir and dropping, creating a rebound effect. We minimised this by leaving a very small gap between the ocean level and the top of the weir. We sometimes wished to include a sloped bed, in order to study grounding lines. We found that leaving even a tiny part of the slope exposed to air had a dramatic and adverse impact upon our experiments (like Robison). We therefore decided to have it entirely submerged, but to guarantee the formation of a sheet and also to reduce the rebound effect just mentioned, the sloped bed was usually placed 2mm below the top of the weir (with the sea level halfway between the top of the slope and the top of the weir, as indicated in Figure 3). Maintaining this configuration required accurate control of the sea level.

We achieved this by means of a laser reflecting off the ocean surface onto a fixed screen. Water was siphoned out at a variable rate, with manual adjustments to this rate whenever necessary to keep the laser spot at the same location on the screen. We found that the rate of seawater extraction could be altered by 0.2g/s, so we could easily control it accurately enough for our purposes. It is likely that the sea level was controlled to within 1mm for most experiments, and 0.5mm for some of them where there were less ripples

on the water (usually due to a lower flux). Therefore, systematic trends in the sea level were small during all of our experiments.

The most probable cause of errors is simply the strong sensitivity of the experiments to initial conditions. Thus, a slight asymmetry (e.g. due to the tank being slightly tilted to one side) can cause loss of contact with the sidewalls at early times, leading to the sort of pattern seen in Figure 5. The finite extent of the experiments also created a finite error on any experimentally determined power law dependence of the parameters on time. This was mostly due to difficulties in determining precisely when the experiment started. Because xanthan would not usually overflow the whole weir at the same time, the flux entering the channel would rise from 0 to  $Q$ . This would cause the front to accelerate. To overcome this problem, we usually waited for the front to stop accelerating and then did a regression. The time at which this regression line passed through 0cm we took to be the time origin for the whole experiment.

Our theory for no sidewall experiments indicates that acceleration not due to rising flux, if present at some time, must also necessarily be present at all later times during the experiment. As the front only accelerated at early times during these experiments, we concluded that this was in fact due to changing flux, and so this must also be the case for similar experiments with additional viscous drag from sidewalls. Thus, all instances of the front accelerating are ascribed to a known artefact of our experimental setup.

Although we consider the procedure perfectly reasonable, it does lead to an error of at least 1 second on the time origin used for the whole experiment, and sometimes as much as 10. Also, the shelf was not usually thickest at the weir itself, but a few cm beyond it. Upstream of here, bending moments were likely having a significant impact upon the flow. As such forces are outside our model, they lead to the model only becoming valid for regions downstream of the point of maximum thickness. This leads to the conclusion that all position measurements should be relative to the point where bending moments become insignificant. Of course, the location of this point has an error of about 1cm (though for very thick shelves, it may be much more). For consistency, though, we would also need to subtract the time required to fill up the section of the profile behind this point. For simplicity, we did neither, believing the effects to be roughly comparable and fairly small in any case. Experiments where this was not so are excluded from our analysis (though we show the data anyway).

Because our procedure essentially assumed no flux entering the channel at all until such time as all  $Q$  was entering the channel, we underestimate the amount of fluid in the channel. This means the experiment effectively got underway earlier than we are assuming, causing us to overestimate the intercepts and underestimate the gradient on the log-log graphs we used. One possible solution is to accurately determine the total amount of fluid which crossed the weir. This could be done if we knew that the sea level had been maintained very accurately and measuring how much water had to be extracted to achieve this. As soon as the experiment finished, the peristaltic pump could be reversed, to prevent further flow of xanthan into the ocean. Then, the position of the laser spot for sea level control could be compared with its initial position to see how much change there had been. We estimate that the total volume of fluid pumped into the ocean could be determined to within  $40\text{cm}^3$ , corresponding to an error of only a few seconds on the effective start time. However, not realising the importance of it, we did not perform this procedure. These are also excluded from our analysis, but again the data is shown.

Another source of uncertainty was the wavelike oscillations that are evident in the bottom view above. These are due to hydrostatic rebound of xanthan dropping into the ocean from a finite height. We tried various techniques to reduce the effect of such waves, and were successful in nearly eliminating them. Therefore, only two experiments were significantly affected by this phenomenon.

There are a few more sources of error worth mentioning. Firstly, the concentration of xanthan may have been slightly below 0.5%, because of losses in transferring the powder from the container in which it was weighed into the water. We assume that about 5% of the xanthan may have been lost in this way, meaning the concentration may have been systematically lower (only 0.47%). This will reduce  $\eta_o$  by about 10-15%. Also, the shear rates in our experiments may have been sufficiently low that the power law used to model the viscosity breaks down. Ultimately, the viscosity is not infinite at very low shear rates, so the fluid must be less viscous than we are assuming.

Fluxes were measured by weighing the container from which xanthan was pumped into the tank. Although a slightly different amount may have been overflowing the weir and entering the shelf (especially near the start of our experiments), this is only true for a very short time. The measurements of mass flow rates were very accurate (0.1% or so).

The density of the ocean was measured using a hydrometer, attaining a similar level of accuracy. For xanthan, we put it into saltwater of known density and checked if it floated or sank. When 50% of the samples we put into the water sank, we knew we had the right density. We also checked this using a hydrometer - both gave consistent results, with an accuracy of 0.1% or so on the density. This corresponds to an error of under 2% on  $g'$ . Our density measurements are listed below. We simply extrapolated the density of xanthan at 1% concentration to be 996.

Substance	Density (kg/m <sup>3</sup> )
Water	994
Xanthan at 0.5%	995

The position of the front as a function of time was determined by a MATLAB boundary tracing algorithm. The positions are listed relative to the weir if there was no sloped bed, relative to the point of maximum thickness if this was more than 3cm from the weir and relative to the location of the grounding line if there was a sloped bed. However, experiments in which the position of maximum thickness was more than 3cm from the weir were severely affected by bending moments, making the results of these experiments unusable.

Then we saw if the slope of a graph of  $x_n$  against  $t$  (on logarithmic axes) converged. This is done by requiring the residuals to a linear regression (usually below 0.5%, and sometimes just a tenth of this) to not have a characteristic inverted parabola shape, but to appear essentially random. We list the portion of the tank over which this occurred, and the relevant times. Also listed is the product-moment correlation coefficient, to give an idea of how closely the data fit to a straight line. If an experiment did not converge, then the gradient would still be decreasing by the end of the experiment (because the gradient needs to go down from 1 to  $\sim 0.6$ ). In this case, we did a regression on the last 30 seconds or so of data, to give a bound on what the gradient might eventually converge to, as well as where the intercept could then lie. This equates to an upper bound on the final gradient and a lower bound on the intercept.

Usually, we also excluded data taken in the last 5cm or so of the tank, to allow for the effect of the sea level control mechanism on the shelf. If there was no discernible effect, we used the additional data in our regression. Ocean currents can affect the xanthan because water has a finite viscosity. The effect is almost always to cause a sudden increase in the gradient (on logarithmic axes). However, for very high fluxes, we believe that the change in water pressure favours thickening of the shelf and thus slows it down even further.

If the reader is interested, we strongly recommend manually analysing the (few) photographs from the very end of an experiment (at 8g/s and at 17g/s, to see both regimes). Another interesting thing to try is to exclude the possibility that the effect near the end is part of a long-period wavelike oscillation (we damped these, but they might still be present). This is relatively straightforward - the experiment simply needs to be repeated with the weir moved forwards 10cm or so. That way, the end of the tank would correspond to a different phase of the (hypothetical) wave. We also note that a much more viscous ocean (e.g. using sugar rather than salt to reach the target ocean density) would enhance the effect. However, it was not our intention to understand the influence of ocean currents on ice shelves, so we do not discuss this further.

Our experiments are given between one and three letters and a number to help the reader identify and refer to them. The letters indicate respectively the presence of laterally confining sidewalls, the presence of a sloped bed and the concentration of xanthan used for the experiment.

Letter	Meaning
W	Sidewalls
B	Bed
H	1% concentration used
L	0.5% concentration used

A typical experiment will be identified by e.g. L1 (indicating no sidewalls, no sloped bed and a concentration of 0.5%). The number is self-explanatory. If these do not start at 1 or miss a number, this is because an experiment was excluded from this paper. In this case, a good reason will be given.

Finally, we note that only an error in the concentration of xanthan used (and thus in  $\eta_o$ ) still remains as a systematic effect in the experiments mimicking ice tongues. Other errors for these experiments are purely random, the biggest of which is in measuring the width of the shelf. The thin parts near the edges had to

be excluded from our measurement of  $d$ , for reasons that will become apparent. Such a procedure inevitably creates some error and is partly subjective.

## 5.2 1% aqueous xanthan solution

Experiments with sidewalls were all performed in the same tank with  $d = 0.075m$  (as it was manufactured, the error is negligible). We used  $\rho_w = 1100kg/m^3$  for all WH experiments. Experiments WH1-3 are not included because we were still perfecting our techniques and because the weir had some rust. This severely hampered our experiments because xanthan overflowing the weir tended to stick to the rust rather than flow forwards into the ocean. When the xanthan finally left the weir, it had gone a long way down so there was a huge blob at the front of the shelf. We warn readers attempting to repeat our experiments that they are of an extremely sensitive nature (by most standards), especially those without sidewalls.

We do not include two experiments conducted at an extremely low flux. This is because the shelf was so thin that it lost contact with the sidewalls in a very large number of locations. There was also insufficient sidewall contact to make one experiment converge, although it suggested that the power of  $t$  is  $< 0.56$ . It also suggested a higher intercept than other experiments, although this is almost certainly due to the loss of contact with sidewalls (which reduces the drag on the shelf).

Expt. (WH..)	Flux (g/s)	Convergent power of t	Error	$R^2$	Time (s)	Distance (cm)	Intercept	Error
10	6.23	0.554	0.01	0.9997	216-239	66-70	-3.38	0.06
9	12.41	0.540	0.01	0.9997	101-146	56-68	-3.08	0.06
7	15.18	$< 0.61$					$> -3.30$	
6	7.87	0.541	0.01	0.9997	163-189	60-66	-3.21	0.06
4	3.87	$< 0.61$					$> -3.78$	

Table 2: The results obtained for our experiments with 1% aqueous xanthan solution.

The experiments which did converge were all consistent with each other. Our best estimate for the mean value of the convergent power of  $t$  is

$$0.545 \pm 0.006$$

If  $x_n \propto t^{\frac{n+1}{2n+1}}$ , as predicted by our theory, then we require a value for  $n$  of

$$5.1^{+0.8}_{-0.7}$$

This is entirely consistent with independent measurements of  $n$  for this fluid (which suggest  $n \approx 5$ ).

Next, we check if the intercepts are also consistent with our theory. However, we should not expect them to be. This is because it was obvious that there are significant thickness variations across the channel. As already shown, only a  $X\%$  difference between mean and edge thicknesses can lead to a  $\sim Y\%$  discrepancy between the predicted and measured values of  $u$  (and thus of  $x_n$ ). Considering how easy it was for the shelf to lose contact with the sidewalls altogether, we suppose that there must have been a significant variation in thickness across the channel. Presumably, the wider the channel or the more viscous the fluid, the more difficult it is to transport mass towards the sidewalls. This is essential to making these regions thicken with time (along with the rest of the shelf). We thus predict that a narrower channel should give better agreement with our theory, as should a less viscous fluid.

We now proceed to rescale the intercepts (on a log-log graph) based on changes in  $Q$ , remembering that  $x_n \propto Q^{\frac{n+1}{2n+1}}$ . Once the rescaling is done, the intercepts should (theoretically) all be equal.

As can be seen from Table 3, the values are roughly consistent, although the theoretical value is about -5. Our best estimate for the rescaled value of the intercept is:

$$-4.19 \pm 0.04$$

The discrepancy with our theory could be due to lateral thickness variations and partial loss of sidewall contact throughout the shelf. The scaling of  $x_n$  with  $Q$  appears to be as expected, but the changing relative importance of lateral thickness variations leads to this not being completely correct either. The net effect is that experiments at a lower flux go slightly faster than we would predict from scaling data for a higher flux experiment. Presumably, this is due to lower  $H$  - note only  $Q$  varied between experiments, so  $H$  would have been correlated with  $Q$ .

Expt. (WH)	Flux (g/s)	Rescaled intercept	Error
9	12.41	-4.22	0.06
10	6.23	-4.21	0.06
7	15.18	$> -4.5$	
6	7.87	-4.14	0.06
4	3.87	$> -4.4$	

Table 3: The intercepts obtained for the experiments with 1% xanthan solution, rescaled according to our theory and the alterations in flux. The theoretical value is -4.99, assuming  $n = 5$  and  $\eta_o = 10$ .

Another interesting thing to note is that the impact of lateral thickness variations was very similar for all experiments. This suggests that the fractional variation in thickness across the channel was much the same, so the lateral thickness profile might be self-similar inside and between experiments. Otherwise, the data would not remain parallel to our theoretical solution. Future work may elucidate this further.

The intercepts are given when the data (in SI units) is plotted on a log-log graph (with base 10). The rescaled intercepts are what would be obtained if the scaling predicted by our theory is correct and the flux was reduced to 1g/s (so  $Q = 1.004 \text{ cm}^3/\text{s}$ ).

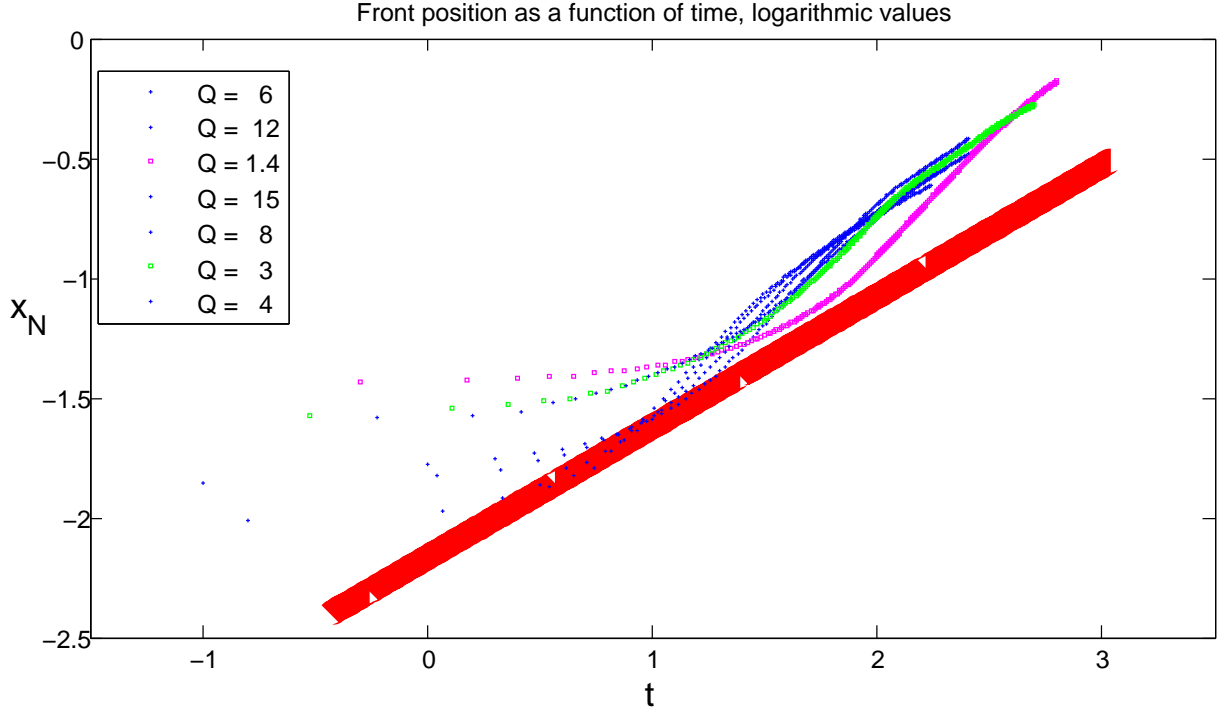


Figure 6: The rescaled raw data for all reliable WH experiments (the most reliable ones are in blue). The experiments at very low fluxes had too much lateral thickness variation to be considered reliable, and they showed the strongest disagreement with theory. All experiments are well above the theoretical line, shown in red. Surprisingly, though, they differ from the theoretical curve by a very similar amount, suggesting the scaling relations with  $Q$  and  $t$  still work.



### 5.3 0.5% aqueous xanthan solution

We attempted to minimise the effects of lateral thickness variations upon the shelf. This can be done by reducing the width of the shelf, but we attempted instead to reduce the viscosity of the fluid by reducing the concentration of xanthan to 0.5%. This reduces the viscosity by a factor of about 3. It also reduces  $n$ , which is highly desirable as ice has  $n \approx 3$ . However, we did not quite reduce the concentration enough to reach this, because if we did then the fluid would not be very viscous and the flow might fail to be at low Reynolds number.

Experiment (WL..)	$\rho_w$	Flux	Convergent power of $t$	Error	$R^2$	Time (s)	Distance (cm)	Intercept	Error
1	1100	6.62	$< 0.61$					$> -3.67$	
2	1100	12.05	0.56	0.03	0.9994	47-163	37-75	-3.14	0.1
3	1100	16.73	0.53	0.03	0.9997	66-123	51-71	-2.9	0.2
5	1100	3.96	0.58	0.02	0.9985	309-350	64-69	-3.77	0.06
B6	1053	11.79	0.57	0.02	0.9986	105-233	42-66	-3.52	0.06
7	1053	12.29	0.61	0.03	0.9993	68-213	41-82	-3.48	0.06
B10	1029	3.9	0.56	0.015	0.9842	420-684	44-57	-4.24	0.06
B11	1100	3.79	$< 0.61$					$> -4.24$	
B12	1100	15.5	$< 0.80$					$> -4.26$	
B13	1029	8.12	0.56	0.015	0.9946	175-387	39-58	-3.88	0.06
B14	1053	15.9	$< 0.67$					$> -3.66$	

Table 4: The results obtained for our experiments with 0.5% aqueous xanthan solution.

We have not included two experiments which had extremely thick shelves, due to bending moments near the weir playing a role over a large section of the tank. Most likely, the correct thing to do is to subtract  $\sim 10$  cm from the front positions, to account for this region (as our theory only becomes valid beyond it). This is also suggested by the fact that, unlike all other experiments, the gradient on a log-log graph (of position against time) was actually increasing (rather than decreasing from 1 at early times towards  $\sim 0.5$ ), strongly suggesting a zero error. However, because we could not precisely determine what correction to use, we do not include such experiments.

Also not included is the first experiment we conducted that had a sloped bed. This was partially exposed to air, which led to an unusual start to the experiment and loss of contact of the shelf with the sidewalls over a 5cm region near the front. Subsequent experiments had a much shallower ( $\sim 10^\circ$  instead of  $26^\circ$ ) sloped bed installed, as well as this being entirely submerged. Contact with the sidewalls was much improved as a result.

Unsurprisingly, the additional length of tank used up by the sheet meant that convergence to self-similar propagation was harder to obtain (although it greatly improved the quality of the experiment). However, we still managed it on three occasions. As the sloped bed did not appear to have a significant effect on the shelf, we treat *all* WL experiments in the same way.

Errors were raised slightly by the lower viscosity of the fluid, which made it more prone to oscillations due to hydrostatic rebound. However, experiments with a sloped bed or with a flux below 7g/s were only slightly affected. This meant that only experiments WL2 and WL3 are noticeably affected. In what follows, we do not use either, because we could not average over enough oscillations.

Our best estimate for the asymptotic behaviour of the shelf is that the front propagates as a power law in  $t$  with exponent

$$0.565 \pm 0.008$$

This will require a value for  $n$  of

$$3.3^{+0.6}_{-0.4}$$

Getting independent values for  $n$  proved difficult. In the end, we found values at lower concentrations of xanthan than we used, and extrapolated them to 0.5%. The value of  $n$  at 0.4% was 3.33, and at 1% it is

close to 5. Also, at 0.2% it is 2.83. Thus, we expect that at 0.5%  $n$  should be about 3.8, making it consistent with our observations. The reference we used was:

[http://projekt.sik.se/nrs/conference/Old%20conferences/conf2003/Course2003/course\\_Taylor%20.pdf](http://projekt.sik.se/nrs/conference/Old%20conferences/conf2003/Course2003/course_Taylor%20.pdf)

The value for  $\eta_o$  we found in a similar way. At 0.2%, it is  $0.57 \text{ Pas}^{\frac{1}{n}}$ . All values of  $\eta_o$  are given in these units. At 0.4%, it is 2.24 and at 1% it is about 10. Thus, we expect a value of about 3.5 at 0.5%. This allows us to check whether the intercepts are also consistent with our theory.

The values of  $\eta_o$  and  $n$  could be verified by e.g. pumping the fluid into a dry Hele-Shaw cell, forming a lateral-shear dominated viscous gravity current. This is already a well-understood situation, so advantage could be taken of this fact. Other more advanced techniques are also possible.

Experiment (WL..)	Ocean density	Flux (g/s)	Rescaled intercept	Error
1	1100	6.62	$> -4.45$	
2	1100	12.05	-4.18	0.1
3	1100	16.73	-4.07	0.2
5	1100	3.96	-4.32	0.06
B6	1053	11.79	-4.31	0.06
7	1053	12.29	-4.29	0.06
B10	1029	3.9	-4.33	0.06
B11	1100	3.79	$> -4.8$	
B12	1100	15.5	$> -5.4$	
B13	1029	8.12	-4.29	0.06
B14	1053	15.9	$> -4.6$	

Table 5: Intercepts on a log-log graph obtained with 0.5% xanthan experiments. These are rescaled so as to be what one would get for an experiment at  $1g/s$  and with  $g' = 1m/s^2$ , using SI units and base  $e$ . The density of xanthan is  $995 kg/m^3$ . The theoretical value is about  $-4.42$ , with an error close to 0.05 (due to the uncertainties in extrapolating data).

The mean value for the intercept that we obtain is:

$$-4.31 \pm 0.03$$

This is slightly greater than the theoretical value of  $-4.45$ . We have already mentioned one possible cause of the discrepancy - errors in the start time. However, although it is a systematic effect, its magnitude will likely be below the error budget quoted above. An error in the concentration of xanthan could also be to blame (a 15% reduction in  $\eta_o$  leads to a 7% increase in  $x_n$ , as could the low shear rates in the experiments. Lateral thickness variations could also account for a further 2% discrepancy. Combining all of these effects, the (relatively small) discrepancy between theory and observations could conceivably be explained.

To test these ideas, the viscosity of the fluid we used, prepared in the same way as for the above experiments; should be measured directly. One possibility is to use a very narrow tank (a Hele-Shaw cell) and have no ocean, using the viscous gravity current theory to determine the viscosity parameters. Also possible is to use the technique outlined to get a better estimate for the start time. Repeating the experiments in a much narrower tank would make the start time clearer, because lateral variations in thickness would be sufficiently small that the area enclosed by the shelf in a photograph would be a good indicator of its volume.

We observed that all experiments without a sloped bed converged over a length scale that is about  $10L$ . This suggests that the length of the flat portion of the shelf is only a tenth of the whole shelf, at the time when further convergence towards our similarity solution is no longer discernible in our data. It is possible to estimate  $L$  from a photograph - the gradient transitions from 0 to that for the similarity solution over a length scale which is roughly the same as our theory predicts (see Figure 8 and note that the shelf is 90cm long). As discussed in Section 4.2, convergence should (and does) take longer in experiments with a sloped bed installed (when considering the length of the shelf only).

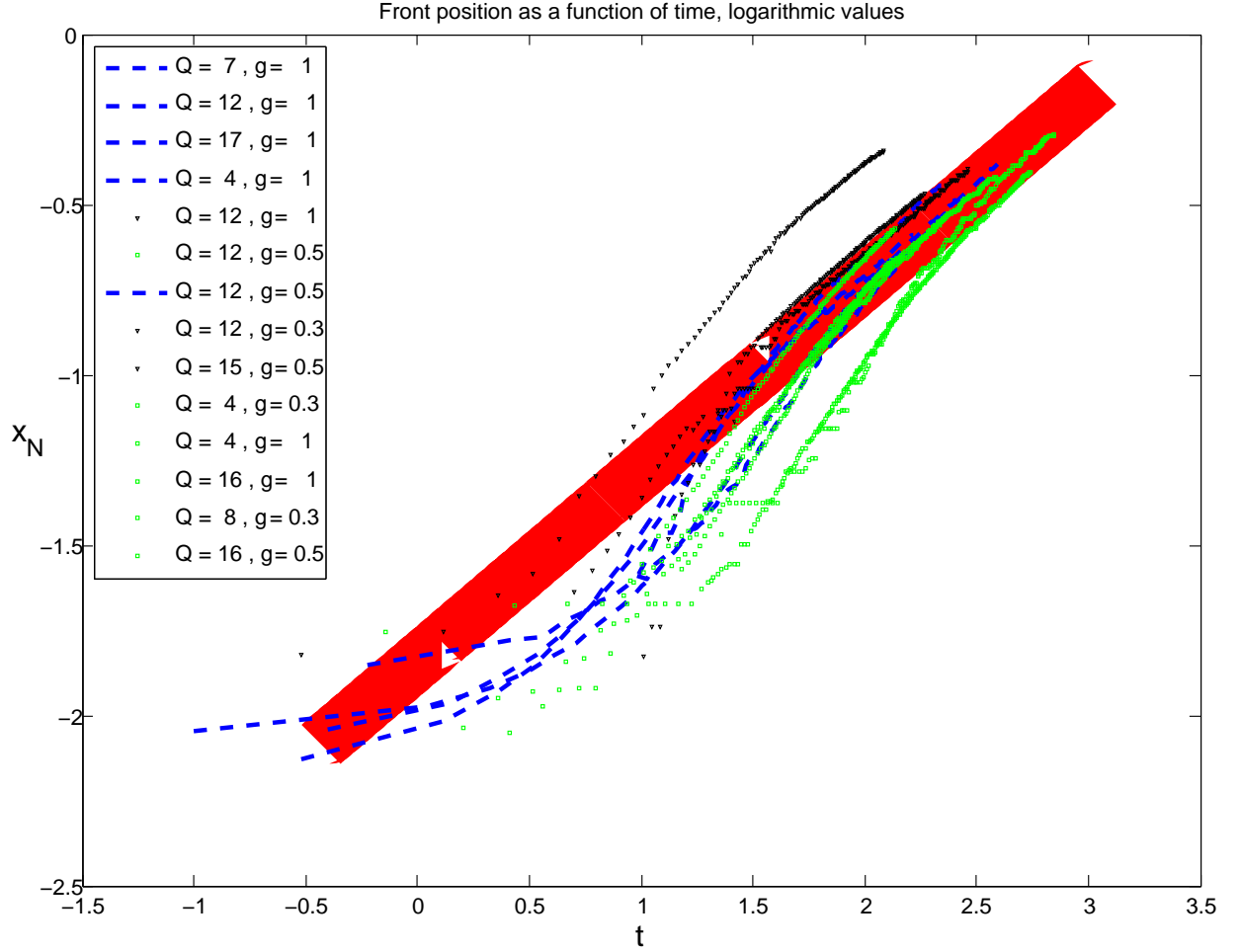


Figure 7: Blue dashes are from experiments without a sloped bed, while green dots are from ones which had a sloped bed installed. All data is rescaled according to how we expect changes in  $Q$  and  $g'$  to affect the shelf. The thick red line is for theory, allowing for some errors. The black curves are from unreliable experiments – we do not use these data when averaging. Note the extended period in all experiments where the gradient is 1, signifying a constant front speed (before sidewalls eventually make it decelerate). This strongly suggests that, without sidewalls, the front would advance at a constant rate.

## 5.4 Thickness Profile

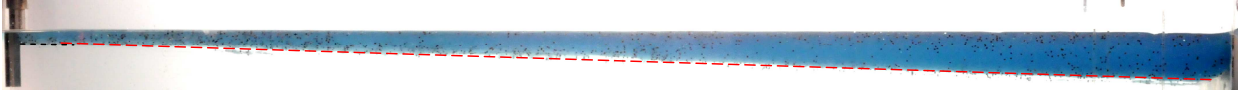


Figure 8: Side view of a sidewall contact experiment (WL1). The dashed red line is drawn to fit the initial gradient of the lower surface of the xanthan. Notice how the shelf is slightly thinner than the red line predicts (i.e.  $|H'|$  rises slightly, as expected). Near the front, the shelf becomes flat. This is because, when this region was near the weir, the theory for ice tongues applied (as there was very little sidewall contact). The region should therefore be nearly flat (or parallel to the black line). Notice that this region is a few cm long (for scale, the shelf is 90cm long) - our equation for  $L$  gives about 3cm. At later times, this region then got pushed along by the self-similar (triangular) region of the profile. Things being ‘pushed along’ in this manner is a characteristic feature of our model, because  $\frac{\partial u}{\partial x}$  is very small.

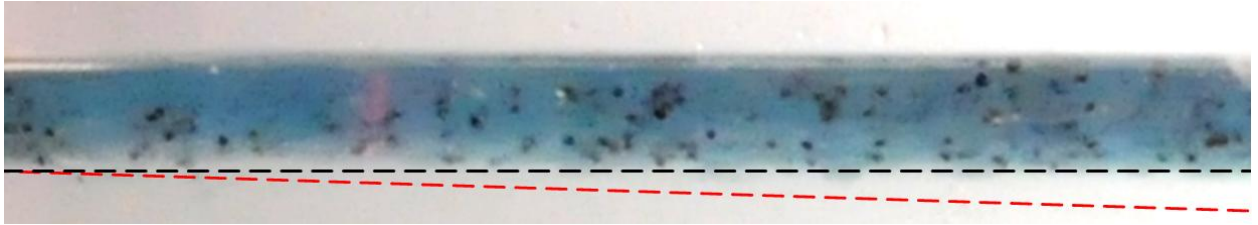


Figure 9: The region near the front (left) in the previous figure is enlarged here. Note that the black line is horizontal, while the red line has the same slope as in the previous figure. As expected, the real profile is not perfectly triangular, with the region shown here in fact being flat. However, this region eventually becomes an insignificant part of the entire shelf, as it doesn’t grow.

## 5.5 Particle Imaging Velocimetry

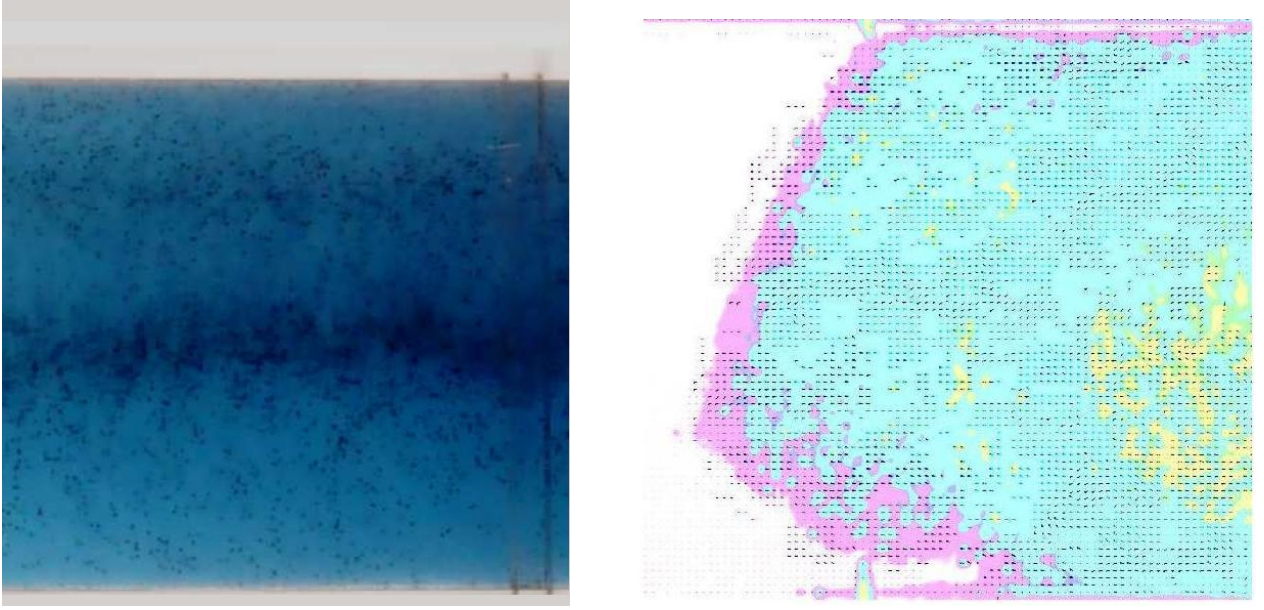


Figure 10: Left: The shelf as it appears in a normal camera, viewed from underneath. Note that the central region is a little thicker, and also has more seeds than other regions. Also note that there was no sheet. Right: Arrows drawn in by DigiFlow as a result of comparing particle positions between frames. The background indicates the thickness of the shelf (it is in false colour).

We attempted to determine directly whether the velocity profile across the channel in sidewall contact experiments was in agreement with our theoretical model. In order to do this, we put in a large number of poppy seeds into the xanthan (about 0.5% by mass). These were almost neutrally buoyant, so vertical motion was negligible during the course of our experiments. We used a high-sensitivity black and white camera with a resolution of  $1024 \times 1024$  pixels to capture photographs at 15 frames per second. Later, we used DigiFlow software to analyse these.

PIV is a relatively new and difficult technique, so we got a relatively large amount of scatter. We therefore averaged over a 20 second period near the end of an experiment which lasted about 200 seconds. The thickness gradient in the shelf goes down as  $t^{-\frac{1}{2n+1}}$ , so we judged that it would hardly change over a 20 second period (and so velocities should hardly change). We also averaged over a 10cm region of the shelf just beyond the point of maximum thickness. Over this region, the change in  $H'$  was minimal (the shelf was about 8 times longer than this, and the shelf is in any case almost perfectly triangular) so  $u$  should hardly vary within it.

The theoretical curve drawn in Figure 11 is based on a maximum speed consistent with the PIV data. Because the fluid is clearly satisfying the no-slip boundary condition, the walls of the tank are clearly visible, 763 pixels apart (this corresponds to 15cm). For the maximum speed, we assume an error of at most 0.5 pixels/second, with a mean value of 12.5. Thus, the maximum velocity is

$$0.246 \pm 0.010 \text{ cm/s}$$

The speed of the front at a time concurrent with these observations is found to be

$$0.27 \pm 0.01 \text{ cm/s}$$

Errors are because the front decelerates during the 20s we averaged over. The theoretical change in  $H'$  between the front and rear of the profile is 2.8%, corresponding to an increase in  $u$  of 11.1% between the rear and the front. This corresponds to a difference in  $u$  of 0.027 cm/s, entirely consistent with our observations.

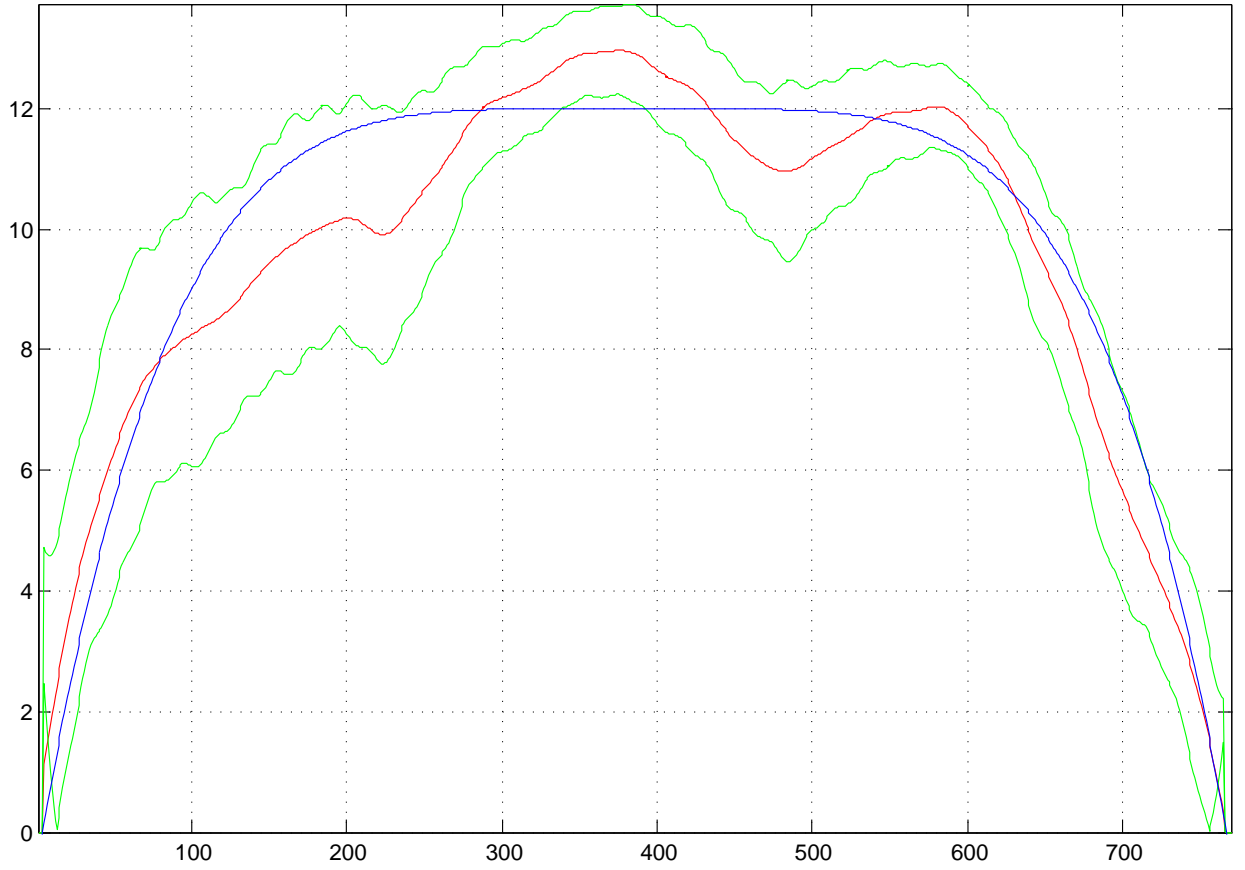


Figure 11: The results of one of our attempts to determine the velocity profile of the shelf. The smooth blue line is for theory. Observations must lie between the jagged green curves (at  $1\sigma$ ), with raw data along the central red curve.

We conclude that both lateral and longitudinal variations in  $u$  are accurately predicted by our theory. We also determined vertical velocity profiles in the sheet, to check whether a viscous gravity current model was accurate. We did this in an experiment with sidewall contact, to increase the thickness of the sheet and get more accurate measurements. Otherwise, only a very small number of particles fit in vertically, despite us using particles sufficiently small that a camera right next to the sheet could only just resolve them.

We expected the viscous gravity current theory to be accurate only for locations sufficiently far downstream of the weir. Therefore, we were expecting to see a discrepancy between theory and observations sufficiently close to the weir.

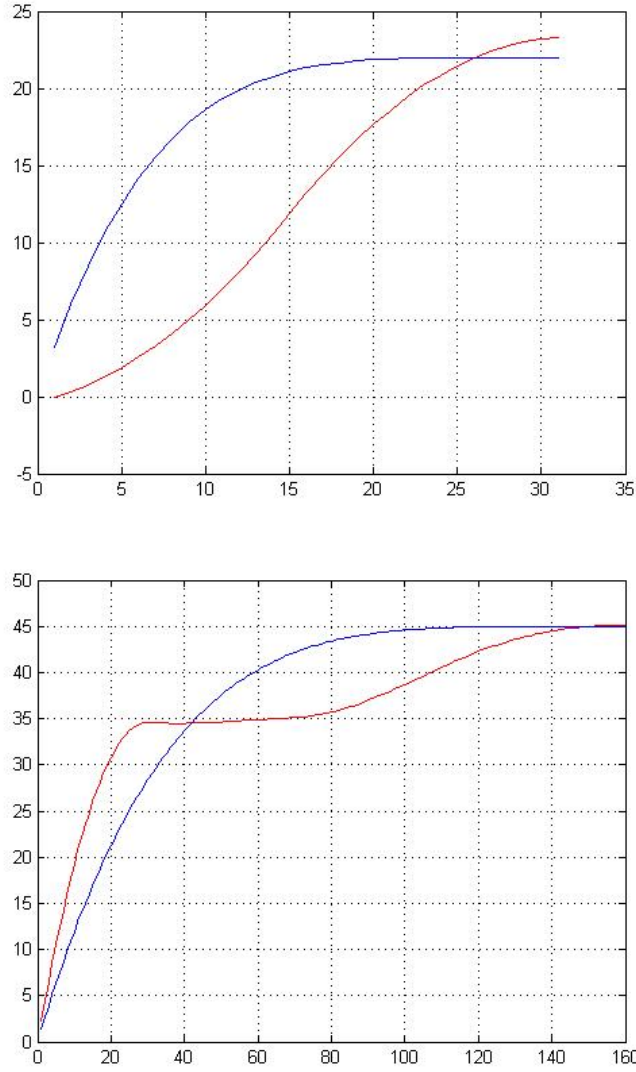


Figure 12: Velocity profiles obtained in the sheet are shown in red, near the weir (top) and further away (bottom). In blue, we try to fit the expected velocity profile for a viscous gravity current, by matching velocities at the top of the sheet. Note that the data are from an experiment with sidewall contact (this should not be important, as the sheet should be vertical shear dominated).

We conclude that the viscous gravity current theory is an accurate description of the situation sufficiently far from the weir, but breaks down too close to the weir. This gives us confidence that we have a reasonable understanding of the sheet, suggesting the grounding line may also have been understood.

## 5.6 No Sidewalls

We also conducted a series of experiments in which the shelf was not in contact with the sidewalls of the tank, at least for a while. The apparatus still looked the same, except for the weir. This now had a groove cut in the central 5cm, reduced to 3cm for the last 2 runs. The groove was just above sea level. For some of the experiments, we installed the sloped bed in the same way as before (i.e. totally submerged and at  $\sim 10^\circ$ ).

The front appeared to go at a constant velocity, except at very early times (when all the flux was not yet entering the shelf). This is consistent with our theory, as the experiments ran for much less time than that required for convergence to a self-similar mode of propagation. Consequently, the front propagated at constant speed. Combined with what appeared to be a constant width to the shelf, we suppose that the grounding line had reached a dynamic equilibrium.

Due to severe technical difficulties, 6 experiments are not shown because the shelf rapidly hit a wall of our tank. Readers attempting to repeat our experiments should note that the inlet and seawater extraction pipes should be (extremely close to) vertical and in the middle of the tank and the whole tank (and any sloped bed inside it) should be level to the horizontal to within about 3 arc-minutes. The sloped bed, which needs to rest against the weir, also needs to have been manufactured to the correct working angle (within a few degrees).

In what follows, we assume that the constant velocity of the shelf can be used to determine the thickness at the grounding line, given also the width of the shelf. One minor complication in measuring the width is that we used the bottom view of the shelf (obviously), whereas the length of the shelf came from the side view. This is because a thin shelf is hard to see from underneath, but it still provides 15cm of optical depth when viewed side on. However, the optical paths are different in the two cases, due to an extra reflection. This means the same physical distance appears as a greater number of pixels in the camera focal plane for the side view.

Errors result from lateral variations in thickness, which make  $d$  hard to determine. These variations were enhanced by the tendency of the fluid to spread sideways without any lateral confinement. We used the colour of the shelf in the bottom view to determine which regions were thin. These regions have been excluded from our measurements of  $d$ .

Also, the grounding line is not at constant thickness laterally (i.e. it isn't a 'line'). This led to a systematic difference between theory and measurements. The reason is that the thick central regions of the sheet at the grounding line, which our theory addresses (because these regions make up most of the sheet), were thicker than the shelf far downstream. Apparently, after the grounding line, the shelf in these regions thins with distance until it becomes roughly the same thickness as the *thinnest* parts of the sheet at the grounding line. Thus, the velocity measurements were essentially indicating how thick the thinnest regions of the grounding line were. This causes the theoretical grounding line thickness (for the thick central regions) to exceed the measured thickness (for the thin regions near the edge). This is an interesting phenomenon, and again a case of lateral structure in the flow outside direct consideration in our model having an influence on the shelf. As before, the effect is more pronounced with a more viscous fluid (more concentrated xanthan).

Our experiments indicated that there was a large amount of lateral spreading in the sheet, mostly very close to the weir (even though the sloped bed was entirely underwater, which we believe reduces the spreading). However, it appeared that there was no noticeable lateral spreading in the shelf. In fact, the spreading appeared to have occurred well upstream of the grounding line in all of our experiments. Combined with the constant speed of the front of the shelf, this strongly suggests a constant thickness.

We attempted to determine directly the thickness of the shelf at the grounding line. The resolution on this was relatively poor, because the thickness is only a few mm in most cases. Thus, it appeared in our photographs as about 20 pixels. Reflections from the ocean and a small amount of parallax made it extremely difficult to perform this sort of measurement (as a look at the photographs will show). The much lower accuracy prevented us from getting a reliable indication of whether our theory is correct using such measurements. However, they did indicate that measurements of  $H_G$  made in this way are consistent with the results of measuring the downstream shelf velocity and width, which we use for testing our theory instead.

Experiments were also conducted without a sloped bed. These indicated negligible lateral spreading, suggesting that ice tongues fed by sheets on steep slopes are unlikely to be much wider than the sheet.





Figure 13: This is a contrast-enhanced photograph of an experiment. The thicker regions appear darker in the bottom view. Note that downstream of the thickest region of the grounding line (in the middle), the shelf actually thins until it is approximately the same thickness as the thinnest regions of the grounding line. The thinning is evident from the side as well (circled region).

We also attempted to understand experiments without a sloped bed. We believe, based on high-resolution photographs, that the angle of the upper surface of the xanthan behind the weir is always close to  $30^\circ$ . Combined with the no penetration condition, we can obtain a velocity profile analogous to those obtained previously for the sheet. The thickness required to drive flux  $Q$  through the weir is then assumed to equal the downstream shelf thickness.

However, it is almost completely certain that other phenomena are critical to understanding the weir. In particular, surface tension has implicitly been included in our model (in terms of fixing the angle of the free surface) but not explicitly in the force balance. This means that we can not expect the predictions based on this theory to be very accurate. On the other hand, it does give the right order of magnitude. Among other things, future work will need to predict an angle of the upper surface close to observed values.

For experiments with a sloped bed, we find good agreement with 0.5% xanthan. At 1%, although there is only one experiment, it is again highly probable that lateral variations in thickness are more pronounced. As these are outside our model, they will lead to a reduction in the accuracy of our predictions.

Expt.	Flux (g/s)	Slope of bed (degrees)	$\rho_w$	$H_G$ (mm, direct image)	Error	$H_G$ (mm, from front)	Error	Prediction	Ratio $\frac{\text{Obs}}{\text{Pred}}$
H1	3.22		1100	6.5	0.7	7.4	0.3	6.4	1.15
H2	10.05		1100	8.4	2.4	9.1	0.8	7.5	1.20
BH3	7.91	9.91	1100	9.4	1.2	10.6	1.0	13.2	0.80
BL4	3.71	8.25	1100	7.2	1.2	6.8	0.5	6.7	1.02
BL5	3.88	8.59	1175	4.3	1.0	6.3	0.5	6.4	0.98

Figure 14: Results obtained from experiments without lateral friction. We have only a very basic understanding of experiments without a sloped bed (the first two listed above). Lateral thickness variations make our model work poorly for BH3. Note the minor impact of the change in  $g'$  between the last two experiments.

The prediction that  $g'$  does not significantly affect the grounding line thickness appears to be borne out by a comparison of experiments BL4 and BL5, the last of which nearly doubled  $g'$  relative to the others. However, both theory and experiments show a slight reduction in grounding line thickness as a result of making the xanthan nearly twice as buoyant.

Another thing we note is that the shelf buckled in one of our experiments. This led to the front alternately hitting one wall and then the other. The reason for this is unclear, but it appears to be due to internal elasticity of the xanthan. We expect that this is unlikely to occur in ice. The buckling had a small effect on the speed of the front, but much smaller than the error in  $d$ , so we do not discuss it further.

We now show that the effect of non-hydrostatic forces from the weir was dissipated against basal friction before the location of the grounding line. Xanthan is assumed to overflow the weir by an amount  $H$ . We assume that forces here are only hydrostatic, but that this gets converted to a non-hydrostatic force on the sheet due to the highly artificial geometry in the situation. Genuine non-hydrostatic forces at the weir may be calculated on the basis of  $h'$  always being approximately  $30^\circ$ . Such forces appear to be negligible in all of our experiments, compared with hydrostatic forces.

The vertically integrated hydrostatic pressure is  $\frac{1}{2}\rho g H^2$ . The basal friction per unit length is  $\eta_o \left(\frac{1}{2} \frac{\partial u}{\partial z}\right)^{\frac{1}{n}-1} \frac{\partial u}{\partial z}$ . We assume that

$$\frac{\partial u}{\partial z} \approx \frac{2\bar{u}}{H} \quad (\text{vertical average indicated}) \quad (60)$$

$$\approx \frac{2Q}{H^2 d} \quad (61)$$

This is an underestimate because the upper surface of the sheet is free so the base must have more than average shear. However, this will not affect the final result much if  $n$  is large. We obtain that the non-hydrostatic force exerted by the supply mechanism will be dissipated over a length scale  $L$ , where

$$L = \frac{\rho g H^{2+\frac{2}{n}}}{4\eta_o} \left(\frac{d}{Q}\right)^{\frac{1}{n}} \quad (62)$$

For  $H$  around 5mm at the weir (as suggested by photographs) in a 0.5% experiment, we get that  $L < 2\text{cm}$ . This corresponds to a grounding line that needs to be at least 4.5mm thick (including an allowance for the sea level being 1mm higher than the top of the slope). We obtain similar conclusions for experiments at 1%, allowing the thickness at the weir to rise to as much as 9mm to account for the greater viscosity. However, the greater viscosity of the fluid also makes it easier for basal friction to dissipate the force exerted at the weir. Thus, noting that  $L$  has been overestimated, we conclude that our grounding lines can not have been significantly affected by the force exerted at the weir. Therefore, a simple viscous gravity current model for the sheet should suffice for determining  $H_G$ .

We also believe it unlikely that realistic natural situations will allow for such unusual configurations as we had in our experiments, especially anything resembling our weir. Therefore, ice sheets can likely be understood solely in terms of hydrostatic pressure gradients balancing basal friction. However, this should be confirmed based on real viscosity parameters and topography.

A final note concerns the unusual corrugated pattern of the edge of the flow in our experiments. This is known to occur in nature. Our understanding is as follows: variations in flux, due to the oscillatory action of our peristaltic pump, lead to variations in the thickness of the shelf at the grounding line, presumably because a higher flux causes the sheet to spread laterally by an increased amount. Because the rest of the shelf essentially moves as a rigid body, the pattern remains permanently imprinted upon the shelf. This may also explain why the front of the shelf tapers - because it crossed the weir when the flux overflowing it was still rising towards  $Q$ .

In natural situations, the effect can be due to seasonal or other changes in the flux entering the ice shelf. We note that the effect did not arise in those experiments in which we did not install a sloped bed. Thus, the effect is likely reduced if the terrain is steeper close to the grounding line. This affects the area in contact with the ocean, which may have important consequences.

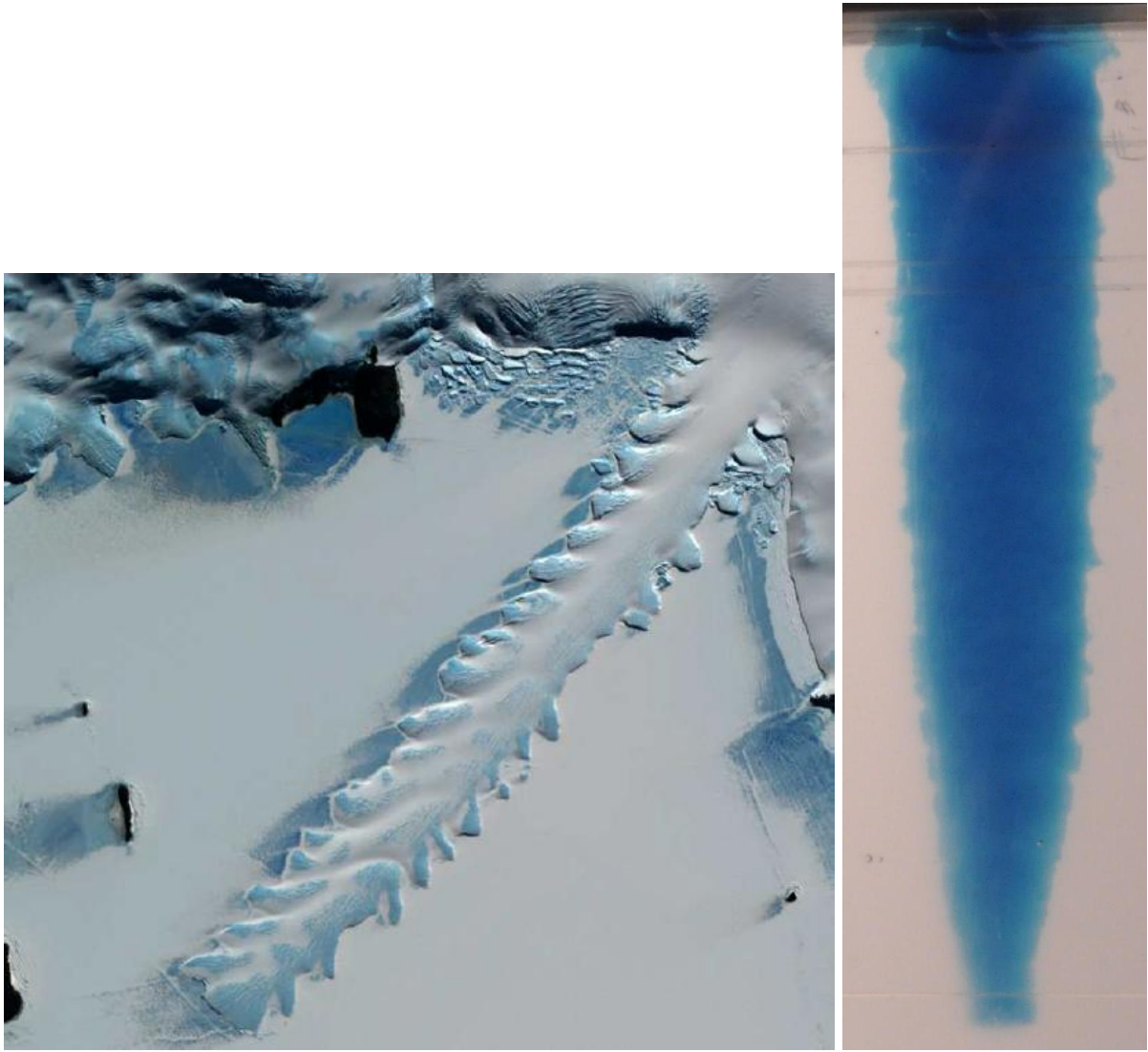


Figure 15: The Erebus ice tongue, showing a similar edge to our laboratory model for such systems. We believe that we have mimicked a seasonal variation in entry flux with the oscillatory action of our peristaltic pump, leading to the similar appearance. Note that our model shelf is much wider than the groove in the weir. This suggests that the shelf determines its own width, this being affected by  $Q$  and likely also by  $g'$ .

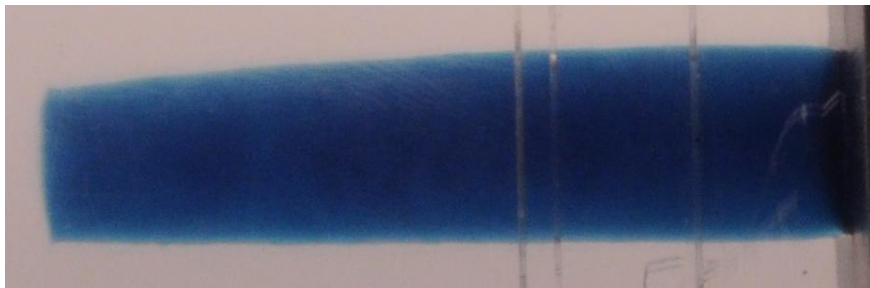


Figure 16: In this run, there was no sloped bed. The corrugations are now absent, although the same pump was used for all of our experiments. The shelf is only as wide as the groove in the weir.

## 6 Conclusions

Recent breakthroughs in understanding the force balance in a simplified laboratory model of a marine ice sheet have now been significantly extended. The theory we developed is valid for the case of a shear-thinning power law fluid, with arbitrary  $n$  (not just for a Newtonian fluid, with  $n = 1$ ). Laboratory experiments confirm that our theory is valid to within the (very tight) experimental tolerances we achieved. The experiments themselves revealed additional aspects of the lab model that are still not fully understood, such as buckling and lateral thickness variations. However, we believe it unlikely that buckling could happen in natural ice shelves, although lateral thickness variations may play an important role.

Our theory for ice tongues is based on a straightforward generalisation of Robison (2010). The equilibrium grounding line thickness is found in a similar way, but the additional complexity means there is no true analytic solution. We do, however, find an approximate analytic solution. The basis for our approximation scheme is that the upper surface of the sheet should be parallel to the lower surface (the bed). This is not always true, so we derive conditions for it to be a reasonable approximation (for ice in water, the bed should have a slope of about  $9^\circ$ ).

For shelves that are laterally confined, our theory is based on the assumption that the fluid undergoes generalised Poiseuille flow. This is true for sufficiently long shelves (assuming they do not lose contact with the sidewalls). We obtain constraints on what length is required, with observations indicating good agreement with our predictions and especially the correct dependence on parameters like the entry flux.

Experiments confirm that the presence of a grounding line does not affect the asymptotic behaviour of laterally confined shelves. Therefore, our prediction for the shelf thickness at its start is equivalent to a prediction of the grounding line position. In this case, an important feature of our solution is that the grounding line advances for ever, although it decelerates.

Future work will need to concentrate on integrating our model for the force balances and the velocity fields they produce with a model for other types of mass transfer. In real ice shelves, melting and snowfall play an important role, but especially crucial is the calving of icebergs at their front. This somehow prevents real ice shelves from thickening for ever, meaning it is of fundamental importance to the shelf (just as much as the force balance is).

Although we have not studied the thermodynamic aspects of glacier systems at all, we believe we have a rough understanding of the effects of ice shelf breakup on the sheet behind it. The cause of the breakup may be rising ocean temperatures. Its effect in terms of causing acceleration of the sheet now appears possible to explain - see Appendix A.

The buttressing exerted by the shelf upon the sheet, which supposedly causes significant acceleration of the sheet if it is removed; actually comes from sidewall contact. If there is no sidewall contact, then the buttressing is equivalent to what would be provided by hydrostatic pressure of water alone, which means this will still be present with no shelf. Only the additional amount due to the shelf being in contact with sidewalls can be removed by melting the shelf, so in ice tongues we do not expect a sudden acceleration if the shelf were to break up. In this case, a reduction in viscosity (due to global warming) may still cause a significant acceleration of the flow (because it is very sensitive to  $\eta_o$ ). However, this is not due to collapse of the ice shelf.

Our model requires assumptions about poorly understood processes like iceberg formation. Detailed understanding of these processes will be essential at some point, if we are to fully understand events like the collapse of the Larsen B ice shelf (nearly ten years ago). Hopefully, these events can be understood in time to prepare for their consequences.

## A The Effects of Ice Shelf Collapse

The effect of an ice shelf collapsing is for the first time partially understood in a way amenable to numerical calculations. We begin by considering the case where there is a bay. In this scenario, the shelf is in contact with the perimeter of the bay (sidewalls). In our theory (Equation 46), constant entry flux into such a shelf leads to it thickening for ever. We suppose that melting and iceberg formation (and possibly sublimation, depending on the temperature) result in the system having a steady profile. Thus, at the grounding line, there will be some surface slope required to drive flux into the shelf corresponding to snowfall over the catchment area of the system. We assume that there is ample time for the system to reach such a state, noting that some of the glaciers have been stable for millennia, if not far longer.

Then, as a result of climate change (perhaps from the resulting change in ocean temperature), the shelf rapidly disintegrates. This step is poorly understood, as it requires a determination of the dominant heat budget in the system, which requires the dominant force budget, which has only just been determined.

The lack of a shelf means the system is now free to settle into a different equilibrium state. The thickness at the grounding line is assumed equal to its previous value, as it will not change significantly over 100 years (this is too little to appreciably alter the enormous thickness of the sheet).

However, the grounding line thickness is fully determined in our model equations, in such a scenario. The lack of a shelf in contact with sidewalls (and the assumption that the sheet is much wider than it is thick) means that the upper surface of the glacier will need to be essentially parallel with the lower surface, in equilibrium. Taking our experiments and observations of nature as a guide, we believe that, initially, the upper surface of the ice sheet is much shallower than this in most cases.

To achieve this increase in slope, the glacier will need to lose some mass. Consider the situation immediately after collapse. Then, in the short run, the flux is still equal to the previous value. As this also corresponds to snowfall, the system is still in equilibrium. However, the equilibrium is now unstable.

Consider a small increase in the flow rate of the glacier. This will lead to a reduction in thickness near the grounding line, but assume that conditions far upstream have not yet been affected. The slope of the surface of the glacier will therefore be increased. This will increase the flux, leading to further increases in the surface slope, and so on.

The situation will be stabilised when the force balance at the grounding line is properly re-established, this time between water pressure alone and the pushing force (previously, although not explicitly shown using our model, forces from sidewalls were affecting the grounding line position by exerting additional buttressing). The situation is now fundamentally different to before, because of the lack of a shelf in contact with sidewalls. This is assumed to occur because we believe that the glacier will prefer to flow into a narrow ice tongue close to the lowest point of the bay (near its centre) rather than to drag along the sidewalls.

We assume that the root cause of this is that conditions are no longer favourable to the ice shelf spreading laterally until contact with the sidewalls is established (because the ice is melted in the time it takes for this to occur). However, it is possible that the ocean is now so hot that an ice shelf can no longer exist, and any ice flowing in is rapidly melted. This leads to a very short shelf and a grounding line close to sea level.

The fact that the system needs to reach a new state of equilibrium with a much steeper surface gradient leads to the observed increase in the flux rate. To get a rough feel, consider our experiments. The grounding line thickness could easily be 30mm, if there is full contact with the sidewalls in a reliable experiment. However, the maximum thickness ever attained in no sidewall experiments is about 12mm, and usually closer to just 7mm. Thus, if we were to impose a constraint that the equilibrium grounding line thickness must equal 30mm, a vast flux rate would be required to sustain this. We assume that at least part of the discrepancy is resolved by a reduction in grounding line thickness, even though this can only ever be a small effect, considering how thick the glaciers are in reality.

The situation in an ice tongue is not prone to this sort of scenario. If the ice shelf rapidly disintegrated, then the grounding line thickness would remain (temporarily) unaltered. However, the equilibrium grounding line thickness is equal to the actual grounding line thickness, so there is no tendency for further change. Assuming also that the resulting flow rate is equal to snowfall over the catchment area of the glacier system, which is likely to occur over long periods of time prior to industrialisation; there will be no corresponding increase in sea level. Indeed, it is unlikely that the ice shelf would ever disappear, for in this model it rapidly re-establishes itself in such a scenario. Also, an alteration in its length does not affect the flow rate (as the buttressing is dependent only on  $H_G$ ). However, reducing  $\eta_o$  in an ice tongue (e.g. due to it getting hotter)

will increase  $Q$  if the grounding line thickness remains constant.

Finally, for shelves in contact with sidewalls, we note that a reduction in the viscosity of the ice due to higher temperatures may make it easier for ice in the shelf to spread laterally and maintain proper sidewall contact. This may delay the collapse of the shelf, because sidewall contact tends to increase its thickness. This effect is likely to be particularly important in wide shelves with low fluxes, where the lateral spreading assumed in this work is likely to be fairly inefficient. An increased flux will also help. Needless to say, with high enough temperatures, sidewall contact and the buttressing this provides will ultimately be lost.